Journal of Theoretical Biology 340 (2014) 251–266

Contents lists available at ScienceDirect

Journal of Theoretical Biology

journal homepage: www.elsevier.com/locate/yjtbi

Leaf hydraulics I: Scaling transport properties from single cells to tissues ☆

Fulton E. Rockwell [a,*], N. Michele Holbrook [b], Abraham D. Stroock [a]

[a] School of Chemical and Biomolecular Engineering, Cornell University, Ithaca, NY 14853, USA
[b] Department of Organismal and Evolutionary Biology, Harvard University, Cambridge, MA 02138, USA

HIGHLIGHTS

- We describe the transport of water through plant cells as a poroelastic medium.
- We show that an approximate theory with the form of the heat equation has an error less than 12%.
- Local chemical equilibrium between protoplasts, cell walls, and adjacent air spaces is sufficient for modeling as a composite.
- Aquaporin mediated cell-to-cell flow dominates isothermal water transport.
- Importance of internal vapor transport for transpiration depends on the temperature gradient.

ARTICLE INFO

Available online 7 October 2013

Keywords:
Poroelasticity
Rehydration kinetics
Plant water transport

ABSTRACT

In leaf tissues, water may move through the symplast or apoplast as a liquid, or through the airspace as vapor, but the dominant path remains in dispute. This is due, in part, to a lack of models that describe these three pathways in terms of experimental variables. We show that, in plant water relations theory, the use of a hydraulic capacity in a manner analogous to a thermal capacity, though it ignores mechanical interactions between cells, is consistent with a special case of the more general continuum mechanical theory of linear poroelasticity. The resulting heat equation form affords a great deal of analytical simplicity at a minimal cost: we estimate an expected error of less than 12%, compared to the full set of equations governing linear poroelastic behavior. We next consider the case for local equilibrium between protoplasts, their cell walls, and adjacent air spaces during isothermal hydration transients to determine how accurately simple volume averaging of material properties (a 'composite' model) describes the hydraulic properties of leaf tissue. Based on typical hydraulic parameters for individual cells, we find that a composite description for tissues composed of thin walled cells with air spaces of similar size to the cells, as in photosynthetic tissues, is a reasonable preliminary assumption. We also expect isothermal transport in such cells to be dominated by the aquaporin-mediated cell-to-cell path. In the non-isothermal case, information on the magnitude of the thermal gradients is required to assess the dominant phase of water transport, liquid or vapor.

1. Introduction

As stomata open to allow an influx of CO_2, the resulting efflux of water vapor must be balanced by the movement of water molecules through the leaf. As a result, apparent leaf hydraulic efficiency (an observed flux divided by an observed water potential difference, a nominal 'conductance') with which leaves transport water correlates with maximum stomatal conductances over a wide range of plants (Boyce et al., 2009; Brodribb et al., 2007). Nevertheless, we lack a clear understanding of the physical bases for the observed differences between leaves in the hydraulic efficiency with which water is delivered to the stomata. Uncertainties about whether the flow path outside the xylem is predominantly apoplastic or symplastic, as well as the relative importance of liquid versus vapor transport within the leaf interior, continue to cloud the question of what determines the maximum transpiration rate observed for a given leaf.

Each of the three different pathways have been presumed by different authors to dominate water transport in well hydrated leaves: the aquaporin mediated cross-membrane flow path (Cochard et al., 2007; Scoffoni et al., 2008), the apoplastic flow path (Brodribb et al., 2007, 2010), and the diffusive path of vapor through the air space

☆This work was supported by the National Science Foundation (award no. DBI 1103664) (F.E.R.), and the Air Force Office of Sponsored Research (award no. FA9550-09-1-0188) (A.S. and N.M.H.).

* Corresponding author. Tel.: +1 914 456 1917.
E-mail address: fulton.rockwell@gmail.com (F.E. Rockwell).

0022-5193/$ - see front matter © 2013 Elsevier Ltd. All rights reserved.
http://dx.doi.org/10.1016/j.jtbi.2013.09.036

(Pieruschka et al., 2010; Mott and Peak, 2011). The lack of consensus regarding the path of transpiration once outside the xylem derives from the inability of current experimental techniques to resolve the individual transport properties of the cell walls, protoplasts, and air spaces within a leaf, or even to measure the actual water potential gradients driving the flux.

One strategy that addresses the latter limitation is to characterize the hydraulic properties of the tissue under non-transpiring conditions, and then, given the known material properties of air, model the competition between liquid and vapor transport within the leaf in satisfying a known transpirational flux. Isothermal transient hydration experiments, which measure the hydration time required for a leaf to transition between two water contents associated with two equilibrium potential states (Brodribb and Holbrook, 2003; Boyer, 1968), can provide the required estimates of leaf tissue hydraulic properties, albeit averaged over the whole leaf. A model of leaf tissue as a composite of protoplasts, cell walls, and air spaces is then needed to parse the tissue hydraulic conductivity into the constitutive hydraulic conductivities of each of these domains. Here we attempt to provide such a model. The related task of incorporating a representation of the xylem network to arrive at a mathematical model of the whole leaf as a tissue irrigated by vasculature is addressed in a separate analysis (Rockwell et al., in submission).

Our goal, as with any porous media approximation, is to find a representation of transport that incorporates the component material properties and their respective volume fractions, but allows us to neglect the details of their geometry within the composite material. To this end, we define a tissue as a composite media, comprising both a liquid phase of living cells and a vapor phase in the intercellular air space. Within the cellular liquid phase, we consider the contribution to hydraulic conductivity and capacity of the apoplast (cell wall space) and symplast (protoplast space) separately. We then use a mixture of mathematical analysis and numerical simulation to find the range of component parameters over which the simple idea of volume averaged material properties provides a description of the bulk behavior equal to that obtained by accounting for transport in each domain separately.

2. Plant tissues as poroelastic media

As far as we are aware, Philip (1958b) was the first to analyze flow through a file of plant cells, in a model later extended by Molz and Ikenberry (1974) to make explicit the contribution from flow in the wall space. As these derivations were somewhat ad hoc, the limitations of the theory were not obvious, although Philip did provide some guidance discussed further below. To better understand the limits of this theory, we begin by reconsidering the transport of an incompressible solvent such as water through a porous and elastic medium, such as an aggregate of plant cells, from the perspective of continuum mechanics. Such a theory was derived by Biot (1941), and is well-described in full by Yoon et al. (2010) and Doi (2009); here we recapitulate some steps to illuminate the limits of Philip's theory in particular, and the physical assumptions latent in the extension of plant cell water relations theory to plant tissues (Table 1).

Given that the physical dimensions of a water absorbing medium change as it swells, as measured in standard laboratory coordinates, it is convenient to adopt a material coordinate system (Gandar, 1983). We label particles $\boldsymbol{x} = (x_1, x_2, x_3)$ according to their position in a reference configuration, and study a material volume

Table 1
Symbol definitions.

Quantity		Value (25 °C)	Units
Area	A	–	m^2
Volume	V	–	m^3
Shear modulus	G	–	Pa
Volumetric modulus	K	–	Pa
Bulk modulus, cell	ε	–	Pa
Water content	C	–	mol m^{-3}
Molecular flux	J	–	mol m^{-2} s^{-1}
Water potential	ψ	–	Pa
Chemical potential	μ	–	J mol^{-1}
Darcy permeability	p	–	m^2
Poroelastic diffusivity	κ	–	m^2 s^{-1}
Cell permeability	L_p	–	m Pa^{-1} s^{-1}
Membrane permeability	P_{os}	–	m s^{-1}
Hydraulic capacity	c	–	mol m^{-3} Pa^{-1}
Hydraulic conductivity	k	–	mol m^{-1} Pa^{-1} s^{-1}
Thermal conductivity	k^T	–	J m^{-1} K^{-1} s^{-1}
Kelvin temperature	θ	–	K
Density of water	ρ_w	9.97×10^2	kg m^{-3}
Molar volume of water	$\overline{v}$	1.807×10^{-5}	m^3 mol^{-1}
Diffusivity, water in air	D_v	2.5×10^{-5}	m^2 s^{-1}
Viscosity of water	η	8.9×10^{-4}	kg m^{-1} s^{-1}
Formula weight of water	f_w	1.8015×10^{-2}	kg mol^{-1}
Heat of vaporization	$\overline{\lambda}$	44×10^3	J mol^{-1}
Gas constant	R	8.3145	m^3 Pa mol^{-1} K^{-1}
Dimensionless variables		**Subscripts**	
Potential	Ψ	Apoplast	a
Time	T	Symplast	s
Poisson's ratio	ν	Cell	c
Transverse strain	ζ	Water, liquid	l
Area fraction	$\mathcal{A}$	Water vapor	v
Volume fraction	$\mathcal{V}$	Initial state	o
Mole fraction	χ	Final state	f
Tortuosity	ξ	Equilibrium	eq

element ($dV = dx_1 dx_2 dx_3$) that tracks a constant amount of dry matter, even as the volume itself shrinks or swells with changing water content. In this conception, an individual plant cell, taken as approximately cubic, becomes an individual volume element. Conservation of molecules requires that the change in the concentration of water molecules C in a material volume be equal to the net flux of water into the volume, or

$$\frac{\partial C(\boldsymbol{x},t)}{\partial t} = -\nabla \cdot \boldsymbol{J}(\boldsymbol{x},t). \tag{1}$$

The Darcy flux of water molecules in response to a gradient in chemical potential, assuming homogenous and isotropic material properties, is given by,

$$\boldsymbol{J} = -\frac{p}{\overline{v}^2 \eta}\nabla\mu(\boldsymbol{x},t), \tag{2}$$

where p is the Darcy permeability with units of m^2, and in the context of plant cells, the flux is in relation to the cellular membranes and walls that are themselves stationary in the material coordinate frame. Eqs. (1) and (2) may be combined,

$$\frac{\partial C(\boldsymbol{x},t)}{\partial t} = \frac{p}{\overline{v}^2 \eta}\nabla^2\mu(\boldsymbol{x},t). \tag{3}$$

We can get (3) into a form more familiar to plant physiologists by defining a hydraulic conductivity k, and recalling the definition of water potential ψ, to arrive at,

$$\frac{\partial C(\boldsymbol{x},t)}{\partial t} = k\nabla^2\psi(\boldsymbol{x},t), \quad k \equiv \frac{p}{\overline{v}\eta}, \quad \psi \equiv \frac{\mu}{\overline{v}}. \tag{4}$$

The steps to this point have been consistent with theory of poroelasticity, as derived from the perspective of thermodynamics and continuum mechanics (Biot, 1941; Yoon et al., 2010). In addition, for small changes in volume, as typically occur in rehydration experiments in tissues above the turgor loss point, we may neglect the difference between material and laboratory coordinates (Hong et al., 2008a). However, we have not specified the relationship between C and ψ, and (4) is still a three dimensional equation, relating a volume change to flow over surfaces normal to x, y, z. The next step in deriving the equations governing poroelasticity would be to consider the balance of mechanical forces in the tissue and the deformation of the 'dry fraction' scaffold, which leads to a set of relations between applied forces, water content, the chemical potential of the permeating water, and the field of stress in the tissue (Doi, 2009).

Alternatively, turning to Philip (1958b) for the simpler perspective based on cell water relations, we could find the relation between water potential and water content for a 'big cell' model of a tissue as,

$$\frac{\partial C}{\partial \psi} = \frac{1}{\overline{v}(\varepsilon+\pi)} \equiv c, \tag{5}$$

where ε is the bulk or volumetric modulus of a representative cell, and π is the osmotic potential in the reference state. We can assign this expression the symbol c, and give it a name, the hydraulic capacity of the cells. The form then adopted by Philip (1958b) for the propagation of turgor in a file of plant cells, in response to a change in source water potential on the boundary normal to x is,

$$\frac{\partial C(x,t)}{\partial t} = k\frac{\partial^2\psi(x,t)}{\partial x^2}, \quad k \equiv \frac{L_p l_c}{2\overline{v}}. \tag{6}$$

Comparison with (3) shows that (6) appears to be a one-dimensional version of the poroelastic equation, with k now defined in terms of the cell length l_c and cell permeability L_p for the case of cell-to-cell flow considered by Philip. Here k arises from 'smearing' the permeability of two membrane and wall sections ($L_p/2$) over the length measured from the center of one cell to the next (l_c) to define a continuum conductivity; dividing by the molar volume simply converts the flux from a volumetric to a molecular basis. The one dimensional form follows from the idea that as long as the principal flux is in x, there is no between-cell flow in y, z, though the cells swell in three dimensions. With these ideas, (6) and (5) can then be combined to find a single equation governing ψ,

$$\frac{\partial C}{\partial t} = \frac{\partial C}{\partial \psi}\frac{\partial \psi}{\partial t} = k\frac{\partial^2\psi}{\partial x^2}, \tag{7}$$

$$\frac{\partial \psi}{\partial t} = \kappa\frac{\partial^2\psi}{\partial x^2}, \quad \kappa \equiv \frac{k}{c}. \tag{8}$$

This definition of c has lead us to an equation, (8), which has the form of the heat equation, with the poroelastic diffusivity κ analogous to a thermal diffusivity in that it arises from the ratio of a conductivity to a local storage capacity. To avoid confusion with molecular diffusion, we will refer to the transport of water molecules in a poroelastic body due to potential gradients as permeation (Hong et al., 2008b). The great advantage of the heat equation form is that given appropriate boundary conditions and initial conditions the solutions are well known (Carslaw and Jaeger, 1959).

However, it should be noted that Philip's definition of c, (5), defines the relationship between potential and water content in terms of equilibrium swelling measurements, and yet we are asking this relationship to hold during *transitions between* equilibrium states. Philip (1958b) was aware of the problem, noting that his use of an equilibrium relationship between water content and potential neglected mechanical (elastic) interactions between cells during the transient. Indeed, Philip cautioned that rigorous justification of (8) might require that the middle lamella does not support stress, such that each cell wall is mechanically independent of its neighbor. For leaf mesophyll cells bordered by extensive air space, cell-to-cell mechanical coupling may indeed be weak and one might justify (8) simply on those grounds. However, this argument is unlikely to apply in epidermal tissues, or the closely packed cells around the vasculature. In between these two limits of purely elastic mechanical interactions and no mechanical interactions between cells lies the possibility of viscous interactions, such that the stresses imposed on a cell by the swelling of its neighbors may be partly relaxed by slippage or 'creep' in their relative positions. Here we focus on the simpler limiting cases of a purely elastic linkage (case 1), versus no mechanical linkage between cells (case 2).

In order to ask what happens if the middle lamella does support elastic stress in a non-trivial way (case 1), we have to return to the more rigorous poroelastic theory of continuum mechanics, from which we departed after equation (4). For the sake of simplicity, we again consider small deformations of a linear elastic material, and therefore neglect the difference between laboratory and material coordinates. Poroelastic theory tells us that because of the mechanical coupling between volume elements (cells), stresses induced by swelling can propagate through a tissue ahead of the swelling front, causing a change in the water potential of the unswollen tissue in advance of any change in water content (Hong et al., 2008a; Doi, 2009). To see this, consider that in poroelastic theory the relationship linking the mean normal stress in a body to the water content (related to the sum of the normal strains) and water potential is given by

$$dC = \frac{1}{3\overline{v}K}d\sigma_{kk} + \frac{1}{\overline{v}K}d\psi. \tag{9}$$

Here K is the volumetric modulus, $\sigma_{kk}/3$ is the mean normal stress, the mechanical pressure exerted on a volume element (or by analogy a cell) by its neighbors. For a freely (without external

constraints) swelling sheet of tissue, at equilibrium the normal stresses are again zero, and $dC_{eq} = (1/\bar{\nu}K)\, d\psi_{eq}$. This relation says that the equilibrium swelling behavior is a function of just one parameter, K, which plays the same role for tissues as the quantity $\varepsilon+\pi$ does for cells. However, during the transient the field of stress is generally not zero, and the water potential of the permeating fluid is a function not just of the local water content (i.e., volume), but of the local deformation (i.e., shape) as well, as illustrated in Fig. 1 (adapted from Doi, 2009).

To describe the local deformation, the balance of forces that describes the field of stress in x, y, z must be considered in addition to conservation of mass, and the equation governing the evolution of the water potential field can be shown to take the more complex form (Doi, 2009; Yoon et al., 2010)

$$\frac{\partial \psi}{\partial t} + 4G\frac{d\zeta}{dt} = \frac{3(1-\nu)\bar{\nu}K}{1+\nu} k \frac{\partial^2 \psi}{\partial x^2}. \tag{10}$$

The second term on the left hand side describes the stress due to the change in the strain in the y, z directions ζ, that accompanies swelling propagating along the x direction, where G is the shear modulus, such that during the transient the overall shape of the block is conserved; note that this conservation of shape is not imposed, but emerges from a balance of forces in the tissue (Doi, 2009). On the RHS, we see that two parameters are necessary to characterize the swelling behavior, both K and Poisson's ratio ν, the ratio of transverse (y, z) strain that accompanies an imposed axial (x) strain. For a linear poroelastic body, G, K, ν, are related by,

$$G = \frac{3K(1-2\nu)}{2(1+\nu)}. \tag{11}$$

We can now ask under what conditions do we approach Philip's approximation that mechanical coupling between cells is unimportant ($G=0$). From (11) we see that for $G=0$ requires $\nu=0.5$,

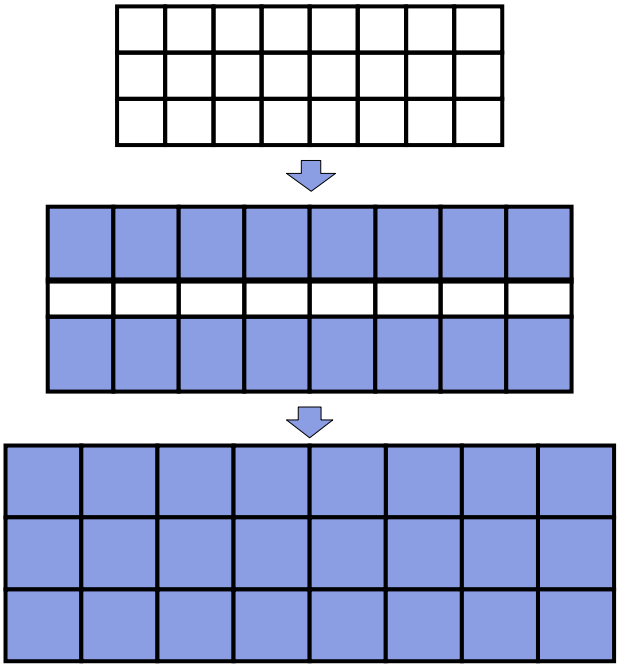

Fig. 1. Free swelling of a plane sheet of tissue, from an initial unswollen (white) state to a final swollen (shaded, or blue (online)) state. During the transition the overall shape of the block is conserved, and the unswollen cells in the center must change shape to accommodate the swelling of the outer tissue. To the extent the cells have a preferred shape, the unswollen cells will experience a change in potential that precedes any volume change.

meaning that a change in the shape of a volume element or cell leads to no overall volume change, i.e., no fluid migration. Hence, for this special value of $\nu=0.5$ water potential is function only of the water content, and not the shape of the volume element or cell (n.b., in poroelastic theory, ν is an apparent Poisson's ratio that results from fluid migration; instantaneously, both the fluid and the dry fraction are considered incompressible. For an illustrative physical example of this idea see Yoon et al., 2010). Inserting $\nu=0.5$ into (10) and (11), we find

$$\frac{\partial \psi}{\partial t} = \bar{\nu}Kk\frac{\partial^2 \psi}{\partial x^2}, \quad \left(\frac{dC}{d\psi}\right)_{eq} \equiv \frac{1}{\bar{\nu}K} \equiv c. \tag{12}$$

For the special case that the water potential of the 'cells' is independent of their shape, one dimensional poroelastic flow (1) does indeed collapse to the heat equation form (8), and the local relationship between water content and potential follows the global equilibrium swelling relationship. Although the cells are mechanically coupled, and shape change propagates ahead of volume change during water uptake, there is no effect on the driving force for flow as the cells have no *preferred* shape. Note that this way of arriving at the heat equation (8) differs from Philip's approximation that the middle lamella does not support stress.

However, neither Philip's justification for the heat equation form (no mechanical linkages between cells), nor the assumption of no shape preference for cells that reduces poroelasticity to the heat equation form, are defensible in the literal sense. First, plant cells adhere to one another to form a macroscopic body capable of withstanding gravity; second, plant cells take on a preferred shape based on the orientation of cellulose microfibrils in their walls (Burgert, 2006). What we have gained by finding the relation between the heat equation form and linear poroelastic theory is an analytical basis for evaluating whether the heat equation form still provides a reasonable approximation to the full poroelasitic theory in the case that individual cells have a shape preference ($\nu \neq 0.5$) and the middle lamella supports stress. Based on a mathematical analysis of the structure of the solution to (10) at long times by Doi (2009), it can be shown that the dependence of the dominant term of the solution, the 'longest relaxation time', on the value of Poisson's ratio over the expected range of $\nu = 0.1 \rightarrow 0.5$ that seems appropriate for plant tissues (Niklas, 1992) varies by only 12% (Appendix A).

Such a weak effect of ν on relaxation times has also been suggested for gels based on numerical implementations of linear poroelasticity (Cai et al., 2010). It appears therefore that the heat equation form (8) that follows from $\nu=0.5$ may provide a good approximation for describing the kinetics of changes in tissue water content and potential in plants. Nevertheless, it is unlikely that plant material is ever an ideal isotropic, homogenous linear poroelastic material. Therefore (8) may be best viewed as a leading order approximation, not necessarily realistic in terms of the details of local deformation. In studies of plant water transport, due to methodological constraints (e.g., the metastability of the water in the xylem) material properties such as hydraulic capacitance as well as water potential and volumetric water content are typically averaged over whole organs, such as leaves (Kramer and Boyer, 1995). As long as the whole organ (e.g., 'leaf level') relationship between water potential and water content remains in a linear range (e.g., much of the range above the leaf turgor loss point, Boyer, 1995), we can apply linear poroelastic theory. According to Doi's (2009) analysis of longest relaxation times, we should then be able to adopt the approximation $\nu=0.5$ and so find the heat equation form (8) with an expected error of at most 12%. It is on these grounds that we will adopt the heat equation form of Philip (1958b) as the basis for the description of leaf tissue hydraulics below.

3. Liquid flow in the apoplast versus the symplast

3.1. Thin-walled cells

In deriving a hydraulic conductivity for a population of cells, Philip (1958a) assumed the dominance of cell-to-cell (cross-membrane and plasmodesmatal) flow, neglecting the apoplast. However, we need not assume negligible flow in the wall space to model aggregates of cells as an homogenous material characterized by a single overall conductivity. Previous simulations, employing an electrical circuit analogy, have suggested that as long as a cell is near local water potential equilibrium (LE) with its own wall, simple volume averaging of hydraulic conductivity and capacity to define 'composite' (apoplastic and symplastic) material properties agrees well with numerical simulations of transient flow along parallel paths Molz (1976) and Molz et al. (1979). In this case, the poroelastic diffusivity becomes,

$$\kappa_l = \frac{k_l}{c_l} = \frac{\mathcal{A}_s k_s + \mathcal{A}_a k_a}{\mathcal{V}_s c_s + \mathcal{V}_a c_a}, \tag{13}$$

where $\mathcal{A}$ and $\mathcal{V}$ refer to the area and volume fractions of the two paths, and the subscripts *l, a, s* reference the total cellular liquid phase, apoplast and symplast respectively.

The analyses by Molz, conducted prior to the discovery of aquaporins, assumed that cell-to-cell flow in the symplast occurred primarily through plasmodesmata. Yet the greater limitation of these studies is the lack of a framework for generalizing the analysis of whether local equilibrium could be expected beyond the particular parameter values culled from the literature of the day. Here we account for aquaporin-mediated cross-membrane flow, and investigate the errors associated with the composite description in two stages. First, we undertake a scaling analysis to analyze the structure of the coupled transport problem in thin-walled cells to find three non-dimensional groups of parameters that determine the structure of the solution. Next, we consider four cases based on the relative magnitudes of these groups to identify the conditions favoring close coupling of apoplastic and symplastic potential (LE). Based on one of these parameter groupings, we develop an order-of-magnitude criteria for the assumption of local equilibrium. We then use this criteria to guide a numerical analysis of the parameter values for which the composite description converges with the numerical solution to the coupled set of equations for apoplastic and symplastic flow.

We start by defining thin-walled cells as cells with an individual length l_c much greater than the thickness of their wall, w_a, and expect this geometrical condition, $l_c \gg w_a$, to describe most of the parenchyma inside a leaf (Esau, 1960). Transport cell-to-cell and through the wall can be written in the form of two diffusion type equations describing the propagation of a change in potential accompanying flow in the two paths, coupled by an exchange of water in response to the local water potential difference across the plasma membrane. Beginning with the geometry in Fig. 2, and the condition that $l_c \gg w_a$, the areas and volumes of the two compartments (neglecting terms of size w_a^2 or smaller) are,

$$\begin{aligned} A_s &= l_s^2 \approx l_c^2 - 4 w_a l_c \\ A_a &= l_c^2 - l_s^2 \approx 4 w_a l_c \\ V_s &= l_s^3 \approx l_c^3 - 6 w_a l_c^2 \\ V_a &= l_c^3 - l_s^3 \approx 6 w_a l_c^2 \end{aligned} \tag{14}$$

The subscripts *a* and *s* refer to the apoplastic and symplastic paths respectively, l_c is the length of a cell in the flow direction (middle lamella to middle lamella), l_s is the length of the protoplast, and w_a is the thickness of the cell wall, such that $l_s = l_c - 2w_a$. Conservation of water molecules in the two compartments then can be written as

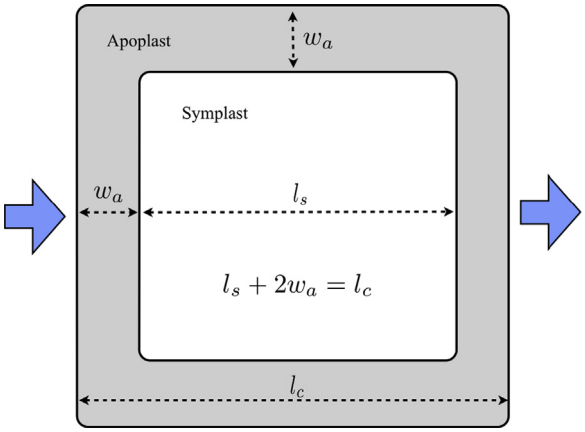

Fig. 2. Dimensions of the symplast and apoplast in the principal direction of flux for an ideal cubic cell.

$$\underbrace{A_s \Delta x\, \Delta C_s}_{\text{accumulation}} = \underbrace{-[A_s J_s|_{x+\Delta x} - A_s J_s|_x]\Delta t}_{\text{change in axial flux}} + \underbrace{4 l_s \Delta x J_{a,s} \Delta t}_{\text{net radial flux}}, \tag{15}$$

$$\underbrace{A_a \Delta x\, \Delta C_a}_{\text{accumulation}} = \underbrace{-[A_a J_a|_{x+\Delta x} - A_a J_a|_x]\Delta t}_{\text{change in axial flux}} - \underbrace{4 l_s \Delta x J_{a,s} \Delta t}_{\text{net radial flux}}. \tag{16}$$

The fundamental theorem of calculus then leads directly to,

$$\frac{\partial C_s}{\partial t} = -\frac{\partial J_s}{\partial x} + \frac{4 l_s}{l_s^2} J_{a,s}, \tag{17}$$

$$\frac{\partial C_a}{\partial t} = -\frac{\partial J_a}{\partial x} - \frac{4 l_s}{4 l_c w_a} J_{a,s}. \tag{18}$$

Note that in writing the exchange terms we have chosen to regard the exchange flux $J_{a,s}$ as positive when net exchange occurs into the symplast. The individual fluxes, with the hydraulic conductivity as the proportionality between the potential gradient and the molar flux, are

$$J_a = -k_a \frac{\partial \psi_a}{\partial x}, \quad J_s = -k_s \frac{\partial \psi_s}{\partial x} \tag{19}$$

$$J_{a,s} = \frac{L_m}{\bar{v}} (\psi_a - \psi_s), \tag{20}$$

where L_m is the permeability of the membrane system between the vacuole and cell wall. For cell-to-cell flow dominated by aquaporins (rather than plasmodesmata), symplastic conductivity comprises the permeability of two protoplasts in series with two wall sections 'smeared' over the cell length,

$$k_s = \frac{L_p l_c}{2\bar{v}} = \left[\left[\frac{L_m l_c}{2\bar{v}} \right]^{-1} + \left[\frac{k_a l_c}{2 w_a} \right]^{-1} \right]^{-1}, \tag{21}$$

where L_p is the permeability of a cell including its wall. This leads to a condition for neglecting the contribution of the wall to cell-to-cell flow,

$$L_m \approx L_p \quad \text{if} \quad \frac{L_m w_a}{\bar{v} k_a} \ll 1. \tag{22}$$

Assuming the above constraint is satisfied, which is not too onerous for small w_a, then the transfer conductance from apoplast to symplast can be approximated,

$$\frac{L_m}{\bar{v}} \approx \frac{2 k_s}{l_c}. \tag{23}$$

To eliminate C_a and C_s from (17) and (18), we need to define the hydraulic capacities that characterize the symplastic and

apoplastic paths. As with k_s above, the capacity of the symplastic path, which we call c_{sp}, has a small contribution from the abutting walls that separate two adjacent protoplasts;

$$c_{sp} = \frac{V_s}{V_{sp}} c_s + \frac{2l_s^2 w_a}{V_{sp}} c_a = \frac{l_s}{l_c} c_s + \frac{2w_a}{l_c} c_a \tag{24}$$

However, as plant tissues decline in volume, losses of water from cell walls are thought to be negligible relative to losses in volume from the symplast (Kramer and Boyer, 1995), or $l_s^3 c_s \gg 6 l_s^2 w_a c_a$, and therefore $l_s c_s \gg 6 w_a c_a$. We then neglect the contribution of the wall sections, and take $c_{sp} \approx c_s$. Substituting c_s and c_a into (17) and (18) brings us to two equations in terms of ψ and t,

$$\frac{\partial \psi_s}{\partial t} = \frac{k_s}{c_s} \frac{\partial^2 \psi}{\partial x^2} + \frac{8 k_s}{c_s l_c l_s} (\psi_a - \psi_s), \tag{25}$$

$$\frac{\partial \psi_a}{\partial t} = \frac{k_a}{c_a} \frac{\partial^2 \psi}{\partial x^2} - \frac{2 k_s}{c_a l_c w_a} (\psi_a - \psi_s). \tag{26}$$

In order to study the structure and behavior of these two equations, we take the standard step of re-scaling to dimensionless variables, with the goal of assessing the relative importance of the individual terms (Deen, 1998). To this end, we re-scale potential and the spatial coordinate to new variables that range from zero to one,

$$\Psi = \frac{\psi - \psi_\infty}{\psi_o - \psi_\infty}, \quad \frac{x}{L} = X, \tag{27}$$

where ψ_∞ is the potential of some source at $x=0$, ψ_o is the initial potential of the tissue, L is the length of the cell file, and n the number of cells, such that $L = n \cdot l_c$. We next re-scale time by a characteristic time τ, with units of seconds,

$$\frac{t}{\tau} = T. \tag{28}$$

This completes the step of introducing dimensionless variables. Note that at this point we do not know yet what τ is; instead we will let the process of making each *term* dimensionless determine the characteristic time scale. Substituting the new variables into (25) and (26) yields,

$$\frac{\partial \Psi_s}{\tau \, \partial T} = \underbrace{\frac{k_s}{c_s L^2}}_{\tau_s^{-1}} \frac{\partial^2 \Psi_s}{\partial X^2} + \underbrace{\frac{8 k_s}{c_s l_s l_c}}_{\tau_{s,a}^{-1}} (\Psi_a - \Psi_s), \tag{29}$$

$$\frac{\partial \Psi_a}{\tau \, \partial T} = \underbrace{\frac{k_a}{c_a L^2}}_{\tau_a^{-1}} \frac{\partial^2 \Psi_a}{\partial X^2} - \underbrace{\frac{2 k_s}{c_a l_c w_a}}_{\tau_{a,s}^{-1}} (\Psi_a - \Psi_s). \tag{30}$$

From (29) and (30) we can identify four candidate time scales that characterize the problem: the characteristic times for changes of potential to propagate along each path independently (τ_s, τ_a), and the characteristic times for potential change in each domain due to transfer of water from the other ($\tau_{s,a}, \tau_{a,s}$).

Here we choose $\tau = \tau_a$, which results in three dimensionless groups,

$$\frac{\partial \Psi_s}{\partial T_a} = \underbrace{\frac{k_s c_a}{k_a c_s}}_{\mathrm{I}} \underbrace{\frac{\partial^2 \Psi_s}{\partial X^2}}_{\mathrm{O(1)}} + \underbrace{\frac{k_s c_a}{k_a c_s} \frac{8 L^2}{l_c l_s}}_{\mathrm{II}} \underbrace{(\Psi_a - \Psi_s)}_{0 \to 1} \tag{31}$$

$$\frac{\partial \Psi_a}{\partial T_a} = \underbrace{\frac{\partial^2 \Psi_a}{\partial X^2}}_{\mathrm{O(1)}} - \underbrace{\frac{k_s}{k_a} \frac{2 L^2}{l_c w_a}}_{\mathrm{III}} \underbrace{(\Psi_a - \Psi_s)}_{0 \to 1} \tag{32}$$

Group I represents the efficiency of potential relaxation through the symplast relative to through the apoplast, which is order one, hereafter, O(1), by our construction. Group II represents the relaxation of the symplast by the adjacent apoplast, and III the tensioning of the apoplast by the adjacent symplast. However, the importance of these transfer processes, relative to transport within a compartment, depends also on the potential difference $(\Psi_a - \Psi_s)$, which may range from zero to one.

Note too that although the spatial derivatives are both O(1), the magnitudes of the time derivatives are not, and are instead set by the need to balance the RHS of each equation. That is, we do not know how many 'T' it takes for Ψ to go to Ψ_∞ in either the apoplast or symplast; it depends on the magnitudes of the parameter groups I, II, III and the difference in potential between the two domains. We can now organize the behavior of the coupled equations with regard to whether the apoplast–symplast potential difference tends toward one or zero (i.e., LE) into five cases, based on whether I, II, and III are each much more or much less, or about the same, as one.

Case 0: $\mathrm{I} \approx 1$. If group I is about one, then potential relaxes at the same rate in both domains, and $(\Psi_a - \Psi_s) \to 0$: local equilibrium holds by definition, and we can write a composite transport equation in terms of a single poroelastic diffusivity summing area and volume weighted conductivities and capacitances.

For the remainder of the possibilities, we can ask which poroelastic time scale is faster (i.e., how large group I is), and then consider the efficiency of transfer between compartments relative to transport within them (the size of II and III). Note that the groups I and II differ only by a geometrical factor that has to be large, meaning that in the symplast, potential change due to transfer out will always be fast relative to potential change due to transport within. The cases we need to consider are thereby reduced to four, based on the behavior of groups I and III:

Case 1: $\mathrm{I} \gg 1, \mathrm{III} \gg 1$: Propagation of potential changes within the symplast is faster than in the apoplast, and, within the apoplast, potential changes due to transfer is more important than diffusion. As a result, apoplastic potential is a slave to symplastic transport—it just contributes capacitance to the governing equation, slowing down the kinetics from what would be expected for the symplast alone. LE holds.

Case 2: $\mathrm{I} \gg 1, \mathrm{III} \ll 1$: Again, propagation of potential changes in the symplast is faster than in the apoplast, while the effect of transfer on the time for relaxation in the apoplast is weak. Note that this case requires $c_a \gg c_s \cdot 2L^2/(l_c w_a)$ to satisfy both conditions, which seems unlikely as changes in total cell volume for changes in water potential are typically dominated by changes in the volume of the vacuole, included in the symplastic compartment (Kramer and Boyer, 1995). Efficient transfer slows the symplast to the point that it follows the diffusive time scale of the apoplast. LE holds.

Case 3: $\mathrm{I} \ll 1, \mathrm{III} \gg 1$: Propagation of potential changes in the apoplast is faster than in the symplast, but transfer of potential out of the apoplast is even faster, holding the two domains close together. LE holds.

*Case*4: $\mathrm{I} \ll 1, \mathrm{III} \ll 1$: As in Case 3, propagation of potential changes in the symplast is very slow relative to the apoplast, however transport within the apoplast is much more efficient than transfer out. The kinetics of the two compartments therefore 'uncouple' in time

$$\frac{\partial \Psi_s}{\partial T_a} = \underbrace{\frac{k_s c_a}{k_a c_s} \frac{\partial^2 \Psi_s}{\partial X^2}}_{\sim 0} + \frac{k_s c_a}{k_a c_s} \frac{8 L^2}{l_c l_s} \underbrace{(\Psi_a - \Psi_s)}_{\sim 1} \tag{33}$$

$$\frac{\partial \Psi_a}{\partial T_a} = \underbrace{\frac{\partial^2 \Psi_a}{\partial X^2}}_{\mathrm{O(1)}} - \underbrace{\frac{k_s}{k_a} \frac{2 L^2}{l_c w_a} (\Psi_a - \Psi_s)}_{\sim 0}. \tag{34}$$

The apoplast goes to source potential before it ever sees demand from the symplast, and, from the symplastic perspective, the

entire apoplast goes instantly from $\Psi_o = 1$, to source potential $\Psi_\infty = 0$. LE fails.

With uncoupling, water permeates into the symplast from the apoplast over all six surfaces of a cubic cell, requiring an update to the geometry for the net radial flux in (15). After returning to dimensional variables, the uncoupled governing become

$$\frac{\partial \psi_s}{\partial t} = \frac{k_s}{c_s}\frac{12}{l_c l_s}(\psi_\infty - \psi_s), \tag{35}$$

$$\frac{\partial \psi_a}{\partial t} = \frac{k_a}{c_a}\frac{\partial^2 \psi_a}{\partial x^2}. \tag{36}$$

Recalling the definitions of k_s and c in terms of cellular parameters, given by (6) and (5), and that for a cubic cell $6/l_c$ is the ratio of surface area SA to volume V, (35) becomes,

$$\frac{\partial \psi_s}{\partial t} = L_p \frac{SA}{V}(\varepsilon + \pi)(\psi_\infty - \psi_s). \tag{37}$$

The result is that in Case 4, the entire tissue follows the same kinetics as a single cell. As tissues appear to have at least an order of magnitude longer relaxation time than individual cells, tens of seconds versus seconds (Kramer and Boyer, 1995), the complete uncoupling of Case 4 seems outside the realm of realistic solutions for plant tissue. Nevertheless, leaf tissues are often implicitly assumed to follow first order kinetics, following an ohm's law analogy whereby the tissue is treated as an ideal capacitor (Brodribb and Holbrook, 2003; Scoffoni et al., 2008; Johnson et al., 2009). For the case of hydrating leaves, such a 'lumped capacity' model may yet be justified if cavitation results in the xylem becoming the limiting resistance to flow (Rockwell et al., in submission). However, in general tissues should not be expected to follow the first order kinetics of single resistor–capacitor model.

Instead, for tissues the interesting case appears to be Case 3, for which the critical condition for LE is,

$$\frac{k_s}{k_a}\frac{2L^2}{l_c w_a} \gg 1. \tag{38}$$

The LHS of (38) describes the local leakiness, from apoplast to symplast, relative to permeation through the apoplast; when this leakiness is relatively large the potential of the two compartments converges. In considering the magnitude of this term, it is helpful to note that we can express L as $n \cdot l_c$, where n is the number of cells across which transport occurs. The LHS of (38) can then be estimated as,

$$\frac{k_s}{k_a}\frac{2L^2}{l_c w_a} = \underbrace{\frac{k_s}{k_a}}_{\sim 1}\underbrace{\frac{2n^2}{1}}_{\sim 50}\underbrace{\frac{l_c}{w_a}}_{\sim 100} \sim 5000. \tag{39}$$

The ratio of the conductivities comes from potato parenchyma (Michael et al., 1997), for which $k_s \approx k_a$, 2.8 and 2.7×10^{-12} mol m^{-1} Pa^{-1} s^{-1} respectively. While comparable estimates of k_a appear to be scarce, estimates of k_s from other pressure probe experiments appear to be consistent with the potato data, with k_s on the order of 1.6 and 1.5×10^{-12} mol m^{-1} Pa^{-1} s^{-1} for *Zea mays* and *Tradescantia* leaf epidermal cells (Kim and Steudle, 2007; Ye et al., 2008). For a cell file five cells long, with l_c 25 μm and w_a 0.25 μm, the RHS of (39) evaluates to ~ 5000, which is indeed much larger than 1, and LE seems a good assumption. Yet, estimates of L_p from cell pressure probe experiments, and L_m from protoplast swelling assays, can range over orders of magnitude even in a single plant organ (Kramer and Boyer, 1995; Ramahaleo et al., 1999), and so we must regard $k_s/k_a \sim 1$ as very poorly constrained. We can then ask how small group III can be before LE becomes a bad assumption, such that, more to the point, adopting the composite model leads to large errors. To address this question, we compared the solutions based on the composite description of the poroelastic diffusivity, (13), to numerical solutions of the coupled equations.

3.2. Numerical solutions for thin-walled cells

We solved the coupled equations, non-dimensionalized using the apoplastic poroelastic time scale as in (31), (32), using the partial differential equations solver pdepe in Matlab (Mathworks, Natick, MA, USA). We studied the problem of potential relaxation in a file of cells with an initial uniform potential ψ_o, hydrating at time $t > 0$ from a source of water at constant potential ψ_∞, located at $x = 0$. At $x = L$, an impermeable cuticle provides a 'no flux' boundary. The non-dimensionalized boundary and initial conditions for both the apoplastic and symplastic domains become,

$$\text{source boundary} \rightarrow \Psi|_{X=0} = 0, \tag{40}$$

$$\text{no flux boundary} \rightarrow \frac{\partial \Psi}{\partial X}|_{X=1} = 0, \tag{41}$$

$$\text{initial condition} \rightarrow \Psi|_{T_a<0} = 1. \tag{42}$$

For the sake of comparison to the numerical results, we then sought the solution to the composite problem in terms of the apoplastic time scale $T_a = t/\tau_a$. Starting with,

$$\frac{\partial \Psi}{\tau_a \partial T_a} = \frac{\kappa_l}{L^2}\frac{\partial^2 \Psi}{\partial X^2}, \tag{43}$$

and multiplying both sides by τ_a brings us to,

$$\frac{\partial \Psi}{\partial T_a} = \gamma \frac{\partial^2 \Psi}{\partial X^2}, \quad \gamma = \frac{\mathcal{A}_s \dfrac{k_s}{k_a} + \mathcal{A}_a}{\mathcal{V}_s \dfrac{c_s}{c_a} + \mathcal{V}_a} \tag{44}$$

subject to the boundary and initial conditions above. As an aside, we note that γ shows the mathematical linkage underlying the coincidence of local equilibrium and the composite model. With the geometry considered here, $l_c \gg w_a$, the area and volume fractions of the symplast are much greater than those of the apoplast, and taking $\mathcal{A}_s \approx \mathcal{V}_s$, we find γ is equal to group I in (31). Hence, (44) has the form of the symplast equation (31), excepting the transfer term. This means that if the composite model holds, in the symplast equation the transfer term must be negligible relative to the poroelastic–diffusive term, and since the derivative is O (1) by construction, we find the inequality,

$$\frac{k_s c_a}{k_a c_s} \gg \frac{k_s c_a}{k_a c_s}\frac{8L^2}{l_c l_s}(\Psi_a - \Psi_s). \tag{45}$$

Dividing through by the LHS and using the relation $L = n l_c$ and the thin walled condition $w_a \ll l_c$, leads to,

$$(8n^2)^{-1} \gg (\Psi_a - \Psi_s), \tag{46}$$

which shows the role of cell number in inhibiting potential differences between compartments during transients.

In comparing the composite solution with the numerical results, we need to account for the fact that plant physiologists are currently limited methodologically to equilibrium measurements of plant water potentials. In this context, this means that the only potential that can be measured accurately is the potential of the tissue once all gradients induced by transient flow have collapsed, and the cell file is once again characterized by a single, uniform potential. We therefore integrated the composite solution with respect to X to find the equilibrium potential predicted for the tissue after hydration for t seconds. The solution to (44) is well

known; after integration it becomes,

$$\Psi_c(T_a) = \frac{8}{\pi^2}\sum_{n=0}^{\infty}\frac{\exp(-\lambda_n^2\gamma T_a)}{(2n+1)^2}, \quad \lambda_n = \left(\frac{2n+1}{2}\right)\pi, \tag{47}$$

and, for numerical evaluation, it is generally sufficient to retain only the first ten terms of the infinite series, as the individual terms die off with both increasing n and T (Crank, 1957). The numerical solutions for the apoplast and symplast domains were also integrated over X, and the equilibrium potential of the cell file, as a function of hydration time, found as the volume fraction $\mathcal{V}$ and hydraulic capacity weighted average of the symplastic and apoplastic potentials,

$$\Psi_n(T_a) = \frac{\mathcal{V}_a c_a \Psi_a(T_a) + \mathcal{V}_s c_s \Psi_s(T_a)}{\mathcal{V}_a c_a + \mathcal{V}_s c_s} \tag{48}$$

Fig. 3 shows the relaxation curves with the ratio of the hydraulic conductivities, k_s/k_a, lowered to 0.01 and 0.001, with group III evaluating to 50 and 5 respectively. For the first case (panel A), the composite and numerical solutions follow similar kinetics, and the apoplastic and symplastic domains remain well coupled (inset).

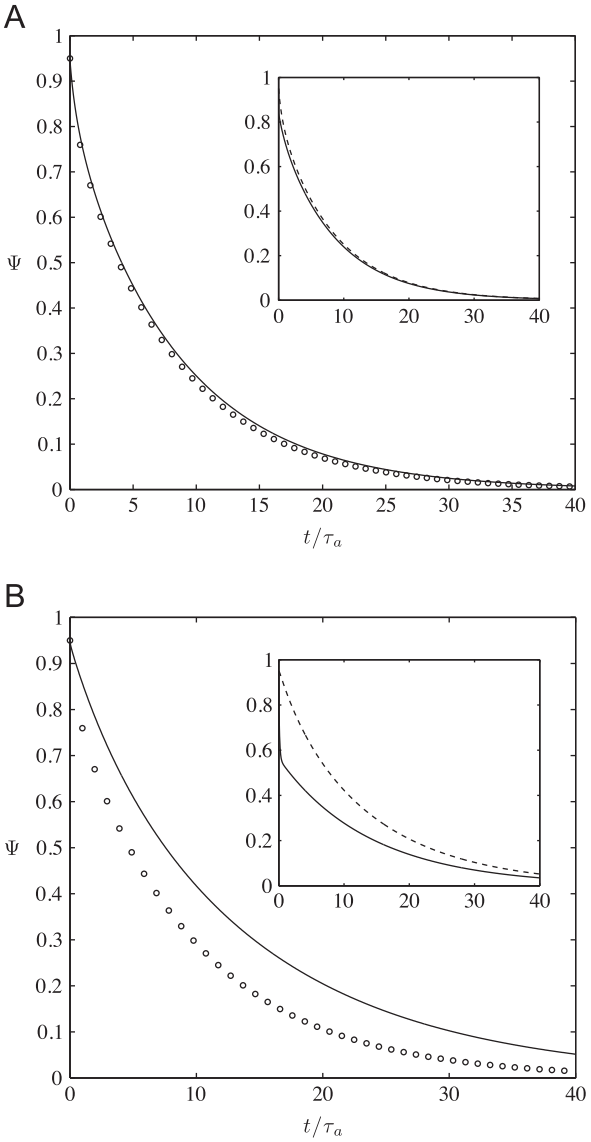

Fig. 3. Tissue potential relaxation curves for $k_s/k_a = 0.01$ (A) and 0.001 (B). Solid line is the numerical solution, open circles the composite model. Insets show the average potentials reached within the symplast (dashed line) and apoplast (solid line) in the numerical solutions.

For the case that group III drops to five (k_s/k_a=0.001, panel B), the composite solution diverges from the numerical, and the difference in the average potential of the symplast and apoplast becomes large, especially at very early times (inset). The initial rapid decrease in the apoplast occurs as it would if it were an isolated domain, which would approach zero by $t/\tau_a = 2$; as the average potential of the apoplast falls while the symplast has yet to change, flow into the apoplast falls even as the amount of transfer-flow to the symplast increases, and the progress of the apoplast toward zero slows.

We can quantify the failure of the composite model, as a function of group III varying from 5 to 50, by comparing the ratio of the halftimes $t_{1/2}$, that is the times at which the composite and numerical solutions predict the cell file will have relaxed to half its initial value. This is an appropriate metric for comparison as rehydration transients in plant tissue are generally fit near the halftime (Brodribb and Holbrook, 2003). The halftime predicted by the composite solution (47) can be found by evaluating the solution for $\Psi_c = 0.5$, retaining a finite number of terms in the series (here, 10), with the well known result $t^c_{1/2} = 0.197\tau_a/\gamma$ (Crank, 1957). The halftime predicted by the numerical solution is by definition $t^n_{1/2} = T^n_{1/2}\tau_a$, where $T^n_{1/2}$ is the solution time T_a at which $\Psi_n = 0.5$. The test of the competence of the composite model is then,

$$\frac{t^c_{1/2}}{t^n_{1/2}} \equiv \frac{0.197\ \tau_c}{T^n_{1/2}\ \tau_a} \equiv \frac{0.197}{T^n_{1/2}\gamma} \approx 1. \tag{49}$$

Fig. 4 shows that the composite halftime is still within 10% of the numerical result for the coupled transport model until group III drops below 20, and that agreement drops precipitously once group III falls below 10. We note that this result is broadly consistent with the result of the scaling analysis that group III should be at leaf an order of magnitude greater than 1 to justify an assumption of LE and the composite model. However, the comparison of halftimes as function of group III provides more specific criteria for adopting the composite model. For example, for an expected error in hydraulic conductivity estimates of less than 10%, Fig. 4 provides,

$$\frac{k_s}{k_a}\frac{2L^2}{l_c w_a} \geq 20. \tag{50}$$

This result means that, with the typical parenchyma geometry considered for the evaluation of group III in (39), even if the estimate of k_s/k_a based on the potato parenchyma Michael et al. (1997) is one hundred times higher than the true typical case, the composite model can still be justified. This is so even though, with this conductivity ratio of $k_s/k_a = 0.01$, the flux through the apoplast is four times that through the symplast. If, on the other

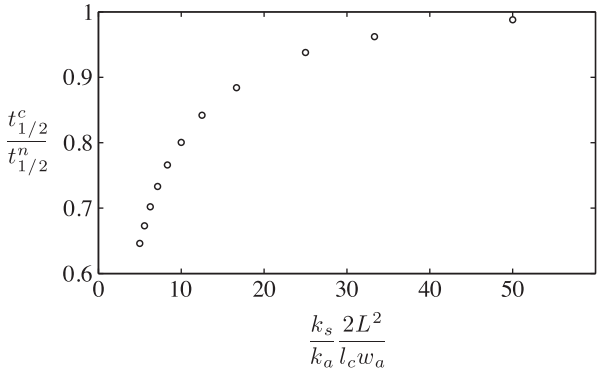

Fig. 4. Ratio of the halftime for tissue relaxation predicted by the composite model to the halftime of the numerical solution, as a function of transfer efficiency relative to apoplastic transport.

hand, the material properties k, c for the symplast and wall space are indeed of the same order of magnitude, then for thin-walled cells the total poroelastic diffusivity (13) will be well approximated by the symplast properties alone, and the diffusivity is well approximated by the form given by Philip (1958b),

$$\kappa_l \approx \frac{L_p l_c(\varepsilon+\pi)}{2}. \tag{51}$$

The advantage of this equation is that it connects the parameter governing tissue behavior (κ_l) to cell-level properties.

The above differs slightly from Philip (1958b) in that the latter includes a shape factor, which represents the proportion of cell-to-cell contact area to cell cross-sectional area. This factor may generally be neglected in the case of experimentally derived estimates of L_p: if cells adjacent to probed cells serve as the sink for flows induced in pressure probe experiments, as it seems they must given the small volume of the adjacent wall space, then such a correction would be already reflected in the experimentally measured values. Yet this raises an issue with the usual interpretation of pressure probe experiments. The relatively small sink represented by a cell's associated apoplast implies that L_p values reported from pressure probe experiments are most likely equal to $L_p/2$ in Philips' model, given that the analysis of pressure probe data typically assumes a sink of constant potential surrounds the cell of interest outside the plasma membrane (Kramer and Boyer, 1995). This assumption, while justified for the algal cells for which the mathematics were originally formulated, likely fails for cells embedded in tissues of thin-walled parenchyma, and we expect that two sets of membranes are crossed in the transient cell-to-cell flow induced by the pressure probe.

3.3. Numerical analysis for thick walled cells

Based on the above arguments, (39) offers strong support for the existence of local equilibrium in aggregates of thin walled cells, such as commonly make up the mesophyll and epidermal tissues of leaves. However, cells packed around major veins may often be thick-walled, and therefore we might question whether the composite model can be expected to adequately describe leaf tissue. To extend our analysis to thick walled cells, we relax the assumption that the radial gradients through the wall are negligible, and model the resulting 3D potential relaxation problem using a finite element analysis software package (Comsol 4.2a, Comsol Inc., Burlington, MA, USA). By symmetry, we study a quarter section of symplastic path and adjacent L shaped wall path for cells with a symplastic length $l_s = 20\ \mu m$, wall thickness $w_a = 10\ \mu m$, through a thickness of 100 μm or five cells; coordinates are then normalized by the longest length for transport, L. The non-dimensional variables are taken as,

$$X = \frac{x}{L}, \quad Y = \frac{y}{L}, \quad Z = \frac{z}{L}, \tag{52}$$

$$\Psi = \frac{\psi(t)-\psi_\infty}{\psi_o-\psi_\infty}, \quad T_a = t\frac{k_a}{c_a L^2}. \tag{53}$$

Substituting (52) into the 3D form of Philip's poroelastic equation (8) provides the non-dimensional form governing transport along the central symplastic path,

$$\frac{\partial \Psi}{\partial T_a} = \frac{k_s c_a}{k_a c_s}\left[\frac{\partial^2 \Psi}{\partial X^2} + \frac{\partial^2 \Psi}{\partial Y^2} + \frac{\partial^2 \Psi}{\partial Z^2}\right], \tag{54}$$

and along the peripheral wall path,

$$\frac{\partial \Psi}{\partial T_a} = \left[\frac{\partial^2 \Psi}{\partial X^2} + \frac{\partial^2 \Psi}{\partial Y^2} + \frac{\partial^2 \Psi}{\partial Z^2}\right]. \tag{55}$$

The boundary and initial conditions are given by,

$$\text{source boundary} \rightarrow \Psi|_{X=0} = 0, \tag{56}$$

$$\text{no flux (epidermis)} \rightarrow \frac{\partial \Psi}{\partial X}|_{X=1} = 0, \tag{57}$$

$$\text{no flux (symmetry)} \rightarrow \frac{\partial \Psi}{\partial Y}\Big|_{Y=1,0} = \frac{\partial \Psi}{\partial Z}\Big|_{Z=1,0} = 0, \tag{58}$$

$$\text{at an interface} \rightarrow \Psi_a = \Psi_s, (J_a - J_s)\cdot\vec{n} = 0 \tag{59}$$

$$\text{initial condition} \rightarrow \Psi|_{T<0} = 1. \tag{60}$$

Fig. 5 shows the numerical solutions to the 3D problem for values of $k_s/k_a = 0.1, 0.01, 0.001$ at their halftimes. For the first two values, the halftimes predicted by the composite model (44) and (47) are within 99% and 94% of the halftimes for the respective numerical solutions, while for the third agreement drops to 82%. For $k_s/k_a = 0.001$, the gradients in the symplast are almost entirely lateral, and the dominant flow into the symplast is through the radial walls. Indeed, even for $k_s/k_a = 0.01$ the 94% agreement in halftimes occurs despite that fact that radial flow appears an important path for hydration of the symplast, and LE is not very well supported. As in the thin walled Case 3, the composite model can provide an apt description of the bulk behavior even when the apoplast is the dominant path for flow.

Finally, considering that in Michael et al.'s (1997) data the *Lp* of cells as measured by the pressure probe as reported is on the order of 10^{-7} m s^{-1} MPa^{-1}, while the range for plant cells is reported to be 10^{-6} to 10^{-8} (Boyer, 1995), then apoplastic and symplastic conductivities may in general be within an order of magnitude of each other ($k_s/k_a = 10 \rightarrow 0.1$), and the composite model justified for thick walled cells as well. At the very least, the presence of thick-walled cells in a tissue should not constitute grounds for rejecting the composite model.

4. Isothermal water vapor transport in leaves

We next consider how to account for the fact that leaf tissues are not just aggregates of cells, but include significant intercellular air spaces, typically 5–50% by volume (Byott, 1976) (Fig. 6). As in considering the symplast and apoplast fractions of the cells, we are again interested in whether we can represent the air and cell volumes as a homogenous medium, whose material properties are again a volume weighted combination of the properties of the two domains, and to what degree success depends on local equilibrium between the two phases (liquid in the cells, vapor in the air space) along axes perpendicular to the principal flux.

To address this problem, it is convenient to express transport in the two phases as a function of a common driving force. Based on the Clausius–Clapeyron equation, and the relation between saturated vapor pressure and water potential (Nobel, 2005), we can write the molar concentration of water molecules per unit volume of air, C_v, in equilibrium with a tissue inhabited by a liquid with water potential ψ at temperature θ as,

$$C_v(\theta,\psi) = C_{ref}\frac{\theta_{ref}}{\theta}\exp\left[-\frac{\overline{\lambda}}{R}\left(\frac{1}{\theta}-\frac{1}{\theta_{ref}}\right) + \left(\frac{(\psi + p_{atm} - p_v(\theta))\overline{v}}{R\theta}\right)\right], \tag{61}$$

where the reference concentration and temperatures are taken as 1.28 mol m^{-3} and 298.15 K. As Clausius–Clapeyron describes the coexistence of the pure phases, and water potential is defined as zero at atmospheric pressure, the liquid 'pressure' dependent term $(\psi + P_{atm} - p_v(\theta))$ is written so that it will be zero (and the effects of liquid pressure on vapor concentration vanish) when the liquid phase has an absolute 'pressure' $(\psi + P_{atm})$ equal to the vapor pressure $p_v(\theta)$.

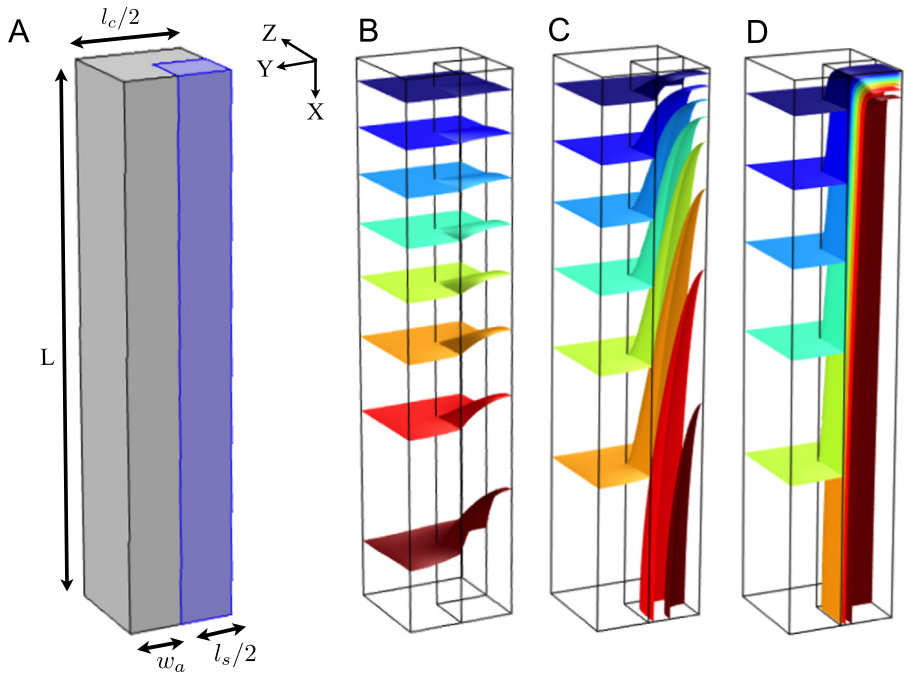

Fig. 5. Isosurfaces for the potential field Ψ at the halftime of transient hydration in a thick walled cell file. (A) Geometry of the cell file; grey is apoplast, blue symplast. (B) $k_s/k_a = 0.1$; (C) $k_s/k_a = 0.01$; (D) $k_s/k_a = 0.001$. Numeric values associated with the color scale (blue = wet, maroon = dry) vary slightly in each case, but by definition the mean Ψ in each case is 0.5. Ratios of the composite halftime to numeric halftime are 0.99, 0.94, and 0.82 respectively. Even for the extreme case of $k_s/k_a = 0.001$, the error in the composite model is only 18%, despite the breakdown in local equilibrium between the symplast and its adjacent wall space.

Following the convention in coupled heat and mass transport of treating the total molar concentration of air C_{air} as constant (Bird et al., 1960), the molar flux of water vapor driven by gradients in the mole fraction of water vapor, χ_v, becomes,

$$J_v = -C_{air} D_v \nabla \chi_v = -D_v \nabla C_v \tag{62}$$

$$= -D_v \left(\frac{\partial C_v}{\partial \psi} \nabla \psi + \frac{\partial C_v}{\partial \theta} \nabla \theta \right). \tag{63}$$

Eq. (61) can be linearized for small variations in temperature of ± 0.5 °C, and potential of ± 1 MPa, with an error less than 0.001 mol m^{-3}. We can then write the linearized form of (62) as

$$J_v = -D_v \left(c_v^{\psi} \nabla \psi + c_v^{\theta} \nabla \theta \right), \quad c_v^{\psi} = \frac{\partial C_v}{\partial \psi}, \quad c_v^{\theta} = \frac{\partial C_v}{\partial \theta}, \tag{64}$$

where c_v^{ψ} and c_v^{θ} are constants found by linearizing the partial derivatives around the temperature and potential that characterize the problem. For the isothermal problem, applicable to rehydration experiments on leaves in thermal equilibrium with their surroundings, $k_v = D_v c_v^{\psi}$ defines the effective hydraulic conductivity of the air space, and c_v^{ψ} describes the capacity of air to store water molecules as vapor. Here we are neglecting the thermal gradients within the leaf that would be induced by the evaporative cooling and 'condensive' heating that must accompany the internal redistribution of water molecules through the vapor phase. However, we expect that for most leaves conduction in the liquid phase is efficient enough that such a thermal feedback on vapor transport will be minimal (Appendix C), and in this 'quasi-isothermal' limit consider the concentration of water vapor in equilibrium with the adjacent liquid phase to be a function of the liquid phase water potential alone.

We can now write isothermal transport within the leaf in both phases in terms of a common driving force,

$$\text{in the air spaces} \rightarrow \frac{\partial \psi}{\partial t} = \frac{k_v}{c_v^{\psi}} \nabla \psi = D_v \nabla \psi, \tag{65}$$

$$\text{in the cells} \rightarrow \frac{\partial \psi}{\partial t} = \frac{k_l}{c_l} \nabla \psi = \kappa_l \nabla \psi, \tag{66}$$

$$\text{at an interface} \rightarrow \psi_v = \psi_l, \quad J_l = J_v. \tag{67}$$

Comparing the diffusivities for the two phases, D^v is on the order of 10^{-5} m^2 s^{-1}, while κ_l, taken as κ_s as estimated from pressure probe experiments, ranges in order of magnitude from 10^{-12} to 10^{-9}, with a consensus value about 10^{-10} (Kramer and Boyer, 1995). This does not mean however that transport through the vapor phase outweighs transport through the tissue. The difference in diffusivities is largely due to the vanishingly small quantity of water it takes to change the potential of the air compared to the tissue; that is, $c_v^{\psi}/c_l \sim 10^{-5}$. As a result, the expected values of both k_l and k_v, the parameters that determine the magnitude of the fluxes, are much closer. For example, at 25 °C, $D_v = 2.5 \times 10^{-5}$ m^2 s^{-1}, $c_v^{\psi} = 9 \times 10^{-9}$ mol m^{-3} Pa^{-1}, and $k_v = 2.3 \times 10^{-13}$ mol m^{-1} Pa^{-1} s^{-1}. This is an order of magnitude lower than k_l values found above. However, data for *Arabidopsis* protoplasts in Morillon and Chrispeels (2001) provide a mean membrane permeability (P_{os}) of 70 μm s^{-1}, for an L_p of 5×10^{-13} m Pa^{-1} s^{-1}, and a k_s of 4.2×10^{-13} mol m^{-1} Pa^{-1} s^{-1} (for the relation between P_{os} and L_p, see Appendix B). Arriving at an expected value for a population of cells is challenging, as the range for individual protoplasts spans an order of magnitude above and below the mean. In addition, in leaves these distributions appear to have a long tail at the high end (Ramahaleo et al., 1999; Martre et al., 2002), and the median value, which may be more important for determining tissue behavior, typically lower than the mean. Thus, while the hydraulic capacity of the gas phase is negligible relative to the cells, transport may not be, with the relative area available for vapor diffusion an important factor. To try to clarify the limits of describing a 1D domain composed of both air and cells with a composite model, we again compare the results of the composite description with a numerical solution for the 3D domain (Comsol 4.2a, Comsol Inc., Burlington, MA, USA).

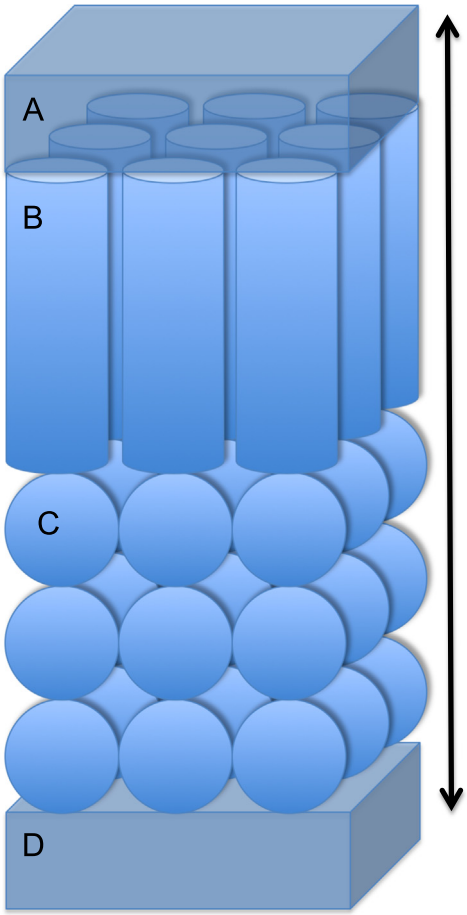

Fig. 6. Schematic showing the general structure of leaf mesophyll and epidermal tissues. (A), (D) Upper and lower epidermis (multicellular). (B) Palisade mesophyll, cylindrical photosynthetic cells organized in vertical files separated by narrow air spaces (anisotropic connectivity between cells). Typically, files may be 1–5 cells thick (1 cell shown). (C) Spongy mesophyll, irregular to globular shaped cells with more extensive air spaces, typically 3–10 cells thick (isotropic connectivity between cells). Arrow shows the principal axis of transport towards the epidermis. A vascular network irrigates the mid-plane between the spongy and palisade mesophyll (not shown).

To simplify the analysis, we rescale the spatial coordinates x, y, z by a length that characterizes transport. Choosing that length again as L, we adopt the new variables $X=x/L, Y=y/L, Z=z/L$, with the resulting domain of interest as in Fig. 7A. To consider transport in a part of a leaf most favorable to vapor transport, we model our domain on a spongy mesophyll with air filled pore space diameters $2R$ twice the characteristic size of the cells $2r$. The later is generous to vapor movement as in the spongy mesophyll of temperate woody leaves air space diameters appear to be about equal to those of the neighboring cells (Wylie, 1939). Symmetry reduces the representative domain of interest to a quarter air space plus an L-shaped region equal to the half thickness of the adjacent cells, and by definition the boundaries normal to Y, Z then have a no-flux condition. We adopt the non-dimensional variables,

$$X=\frac{x}{L},\quad Y=\frac{y}{L},\quad Z=\frac{z}{L}, \tag{68}$$

$$\Psi=\frac{\psi(t)-\psi_\infty}{\psi_o-\psi_\infty},\quad T=\frac{t}{\tau^{3D}},\quad \tau^{3D}\equiv\frac{L^2}{\kappa_l}. \tag{69}$$

Substituting (68) and (69) into (65) and (66) provides the non-dimensional forms of the governing equations for transport through the air space,

$$\frac{c_v}{c_l}\frac{\partial\Psi}{\partial T}=\frac{k_v}{k_l}\left[\frac{\partial^2\Psi}{\partial X^2}+\frac{\partial^2\Psi}{\partial Y^2}+\frac{\partial^2\Psi}{\partial Z^2}\right], \tag{70}$$

and in the cellular space,

$$\frac{\partial\Psi}{\partial T}=\left[\frac{\partial^2\Psi}{\partial X^2}+\frac{\partial^2\Psi}{\partial Y^2}+\frac{\partial^2\Psi}{\partial Z^2}\right]. \tag{71}$$

The boundary and initial conditions are given by,

$$\text{source boundary}\rightarrow\Psi|_{X=0}=0, \tag{72}$$

$$\text{no flux (epidermis)}\rightarrow\frac{\partial\Psi}{\partial X}|_{X=1}=0, \tag{73}$$

$$\text{no flux (symmetry)}\rightarrow\frac{\partial\Psi}{\partial Y}\Big|_{Y=1,0}=\frac{\partial\Psi}{\partial Z}|_{Z=1,0}=0, \tag{74}$$

$$\text{at an interface}\rightarrow\Psi_v=\Psi_l,\quad (J_l-J_v)\cdot\vec{n}=0 \tag{75}$$

$$\text{initial condition}\rightarrow\Psi|_{T=0}=1. \tag{76}$$

The dimensions of the domain of interest in X is then $L/L=1$, the length of the cell file, and $d/L=(r+R)/L$ in y, z. We expect that the larger the length ratio, L/d, the shallower the gradients will be in the y, z planes normal to x; for a representative leaf with a half thickness of 100 μm, a mesophyll cell radius of 10 μm, and an intercellular airspace radius of 20 μm, we take $L=100$ μm, $d=30$ μm, as one might expect for the spongy mesophyll (Wylie, 1939). For the sake of concreteness, we fix the ratio of the hydraulic capacities by considering a red oak leaf for which $c_v/c_l=6\times10^{-6}$. We then ask what happens when the total conductivity to the molecular flux of water is dominated by the cells, is about equal, or is dominated by the air space, and solve for $k_v/k_l=0.1, 1, 10$.

The solution to the 1D composite model has the same form as (47), with the poroelastic diffusivity given by the average conductivity and capacity of the air and liquid sub-domains, weighted by their respective areas and volumes,

$$\kappa_\ell=\frac{k_\ell}{c_\ell}=\frac{\mathcal{A}_l k_l+\mathcal{A}_v k_v}{\mathcal{V}_l c_l+\mathcal{V}_v c_v^{\Psi}},\quad \tau^{1D}=\frac{L^2}{\kappa_\ell}. \tag{77}$$

For a quantitative measure of the effect of neglecting in plane gradients between cells and adjacent airspace, we can again consider the halftimes for transport predicted by the solution to the composite model expressed in terms of τ^{1D}, in relation to that observed for the numerical simulation, for which time is denominated in terms of τ^{3D}. With the above boundary conditions, the halftime predicted by the composite model is $0.197\tau^{1D}$, and the test for the competence of the composite model is just

$$\frac{\tau^{1D}T_{1/2}^{1D}}{\tau^{3D}T_{1/2}^{3D}}\approx1\rightarrow\frac{\kappa_l}{\kappa_\ell}\frac{0.197}{T_{1/2}^{3D}}\approx1, \tag{78}$$

where the unknown $T_{1/2}^{3D}$ is found from averaging the potential field in the cellular domain at each time step of the numerical solution (note that the hydraulic capacity of air is negligible relative to that of the cell fraction, and so the potential in the airspace is immaterial in determining the potential attained by the whole domain as it comes to equilibrium after hydration for t seconds). Fig. 7 shows the iso-surfaces of the potential field in the domain at the halftime given by the numerical simulations. Qualitatively, we can see that for vapor conductivity less than or about equal to that of the liquid path, near local equilibrium is observed between air and cell fractions. Even for vapor conductivity 10 times greater than the cell fraction, the phases do not show too much separation in potential. However, for $k_v/k_l=0.1$, 1, 10, the quantitative test for the composite model based on the ratio of the halftimes, (78), evaluates to 0.999, 0.99,

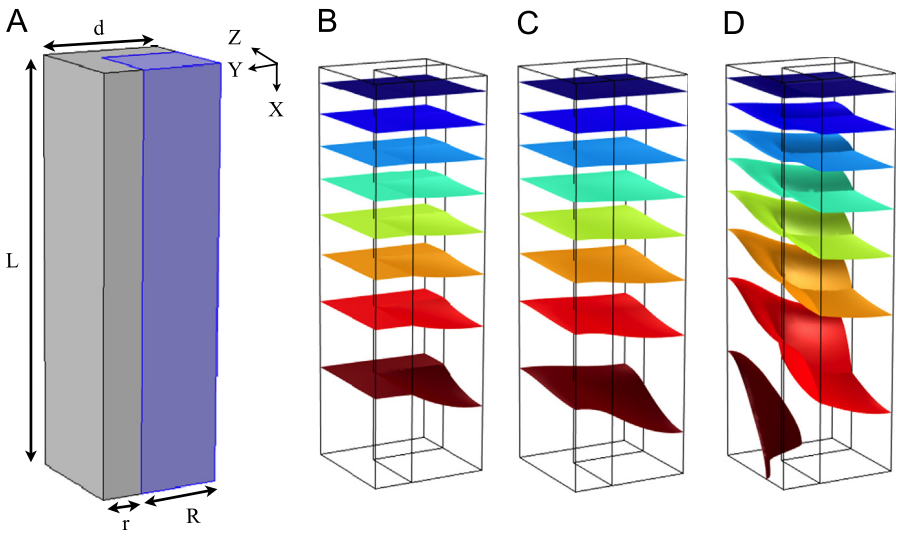

Fig. 7. Isosurfaces in potential Ψ for a tissue composed of cells and adjacent airspace at the halftime of transient hydration through the thickness (X), for three values of k_v/k_l: (A) Geometry of the vapor domain (intercellular airspace) in blue and liquid domain (cells) in grey; (B) $k_v/k_l = 0.1$; (C) $k_v/k_l = 1$; (D) $k_v/k_l = 10$. Numeric values associated with the color scale (blue=wet, maroon=dry) vary slightly in each case, but by definition the mean Ψ in each domain is 0.5. Ratios of the composite halftime to numeric halftime are 0.999, 0.99, and 0.9 respectively. The relatively small hydraulic capacity of the gas phase causes the composite model to significantly overestimate transport for $k_v/k_l > 10$, even as the gas and liquid phases remain near local equilibrium.

0.9 respectively. Thus, for $k_v/k_l = 10$ the error relevant to parameter estimates is already greater than in the thick-walled comparison $k_s/k_a = 0.01$, despite the fact that lateral gradients appear less developed in the vapor than in thick-walled case. That is, despite an apparently close approximation of LE, the composite model can lead to overestimates of transport because it assumes that the high conductivity of the vapor path can directly feed the large sink of the cell fraction; the composite model does not capture the fact that the highly conductive path is limited to the relatively negligible storage capacity of the airspace.

In this test we have taken a very local view of transport just in the spongy mesophyll, a tissue characterized by large air fractions (here, 44%). However, at the whole leaf level air fractions are smaller and therefore we may expect the error resulting from fitting hydraulic conductivities from observed halftimes using the composite model will be lower than estimated here. Furthermore, when k_l exceeds 2.3×10^{-14} mol m^{-1} Pa^{-1} s^{-1} (i.e., $k_v/k_l < 10$), which we expect to encompass most leaves, expected errors even for the 44% air fraction considered here are less than 10%. Neglecting the hydraulic capacity of the vapor phase then leads to a simplified composite model of the form,

$$\kappa_\ell \approx \frac{\mathcal{A}_l k_l + \mathcal{A}_v k_v}{\mathcal{V}_l c_l}. \tag{79}$$

The approximation in (79) arises from the fact that $c_v^\Psi \ll c_l$ for any real volumetric air fraction. Noting that the area fractions in the direction of transport should be about equal to the respective volume fraction, we arrive at

$$\kappa_\ell \approx \frac{k_l + \dfrac{\mathcal{V}_v}{\mathcal{V}_l} k_v}{c_l}. \tag{80}$$

The definition of a composite conductivity as the volume fraction weighted sum of the component conductivities is expected to do well when the component materials are arrayed in parallel in the direction of transport, as for example, would be the case for transport through the leaf thickness within the palisade parenchyma. Where the air and liquid fractions are continuous only along non-linear pathlines, as in the spongy mesophyll, it is customary to ascribe the difference between the observed conductivity and that calculated according to volume fraction to the effect of a tortuosity (Cussler, 1997), to which we give the symbol ξ. In this view, tortuosity accounts for the fact that in substances with heterogeneous material properties transport may not be strictly one-dimensional, depending on the arrangement of the component materials.

As a 'tortuous' bend in a cell file implies a similar bend in the adjacent airspace, it might be assumed that the tortuosity of the two phases must be equal. However, it seems that observed tortuosities can be larger than might be reasonably attributed simply to the increase in path length (Cussler, 1997); that is, the definition of tortuously as the difference between an observation and theoretical expectation makes it a catch-all parameter in which various physical effects may lurk. We thus define separate tortuosities, ξ_v and ξ_l, for the two phases. With respect to the liquid phase, the parameter defined by experiment is the effective conductivity of the liquid path, k_l/ξ_l; only in rare situations is it likely to be possible to arrive at separate estimates of ξ_l and k_l. In contrast, for the vapor phase, the effective hydraulic conductivity, k_v/ξ_v, must be built up from the known material properties D_v and c_v^Ψ, and an independent estimate of ξ_v. In general, tortuosity may be expected to be about three, with a typical range from two to six (Cussler, 1997); in the context of leaf internal air spaces, a value of 1.5 has been suggested (Pieruschka et al., 2005). Accounting for tortuosity, the poroelastic diffusivity of the tissue becomes,

$$\kappa_\ell \approx \frac{\dfrac{k_l}{\xi_l} + \dfrac{\mathcal{V}_v}{\mathcal{V}_l}\dfrac{k_v}{\xi_v}}{c_l}. \tag{81}$$

Eq. (81), together with (13) and (5), completes the description of leaf tissue as a composite media in terms of the constituent material properties of membranes, cell walls, and air.

4.1. Impact of cell size and number on hydration times

We began this analysis by discussing how discrete cellular properties, such as membrane permeabilities and cell size, could be scaled to a continuous property such as hydraulic conductivity. Doing so allowed us to adopt the ideas of continuum mechanics,

and avoid the complexity of a fully discrete description. However, in some cases it may be illuminating to return to the original discrete variables. For example, in the limit that cell-to-cell flow dominates transport, the dependence of the characteristic time τ on cell permeability can be found simply as,

$$\tau_\ell = \frac{c_\ell L^2}{\kappa_\ell} = \frac{c_\ell n^2 l_c^2}{\mathcal{A}_l k_l} = \frac{2}{\mathcal{A}_l} \cdot \frac{\overline{v} c_\ell l_c}{L_p} \cdot n^2. \tag{82}$$

For such tissues, the time for changes in potential or water content to propagate will be linearly related to the characteristic cell size l_c, but will grow as the number of cells n squared. Hydraulic limitation may then arise from the number of cell-to-cell transitions, rather than linear distances, and $n \cdot l_c$ may be a more useful variable than L in analyzing internal leaf structure. The steady state conductance K_n for transport over n cells is then,

$$K_n = \frac{\mathcal{A}_l L_p}{2\overline{v} n}. \tag{83}$$

Notably, (83) emphasizes that, in the limit that tissue conductivity is dominated by membrane permeability, cell number, and not actual tissue dimensions, may provide the most informative measure of how far a cell can be from the vasculature before transport limitations become too great. For example, the relatively low value of k_s calculated here for *Arabidopsis* may be explained by its small cell size, $l_c = 30\,\mu m$, while its mean L_p falls within the range of the other species discussed ($2–7 \times 10^{-13}$ m Pa^{-1} s^{-1}).

5. Discussion

5.1. Poroelasticity and plant water relations

It will be noted that in considering the permeation of water molecules through plant tissues from the perspective of poroelastic theory, we have nevertheless arrived at the same mathematical form as Philip (1958b), and so it might be argued the extra effort was superfluous. However, the exercise did make explicit the approximations and limitations entailed by the use of the heat equation to describe water transport in elastic tissues, and therein lies some of its value. The rest of the value lies in pointing plant physiologists towards a well developed body of theory linking stress, strain and the chemical potential of water at the tissue level, a linkage currently absent in canonical plant texts, such as Niklas (1992), Nobel (2005), and Kramer and Boyer (1995). This absence reflects a lingering confusion on the relationship between descriptions of plant tissue from the perspective of solid mechanics versus that developed in plant cell water relations by treating a tissue as analogous to a single 'big cell'. For example, Cosgrove (1988) pointed out that the bulk modulus ε of cell water relations could not be identified with the volumetric modulus K of solid mechanics, as water must flow out of a cell for it to change volume, while K describes a mass conserving change in volume. In poroelastic theory this difficulty is resolved, for K, G, ν link deformation not just to an imposed state of stress, but to the migration of the fluid as well, while within a volume element only the solid fraction is conserved and the water content varies (Biot, 1941; Hong et al., 2008b). As a result, as we have shown, the poroelastic volumetric modulus K is indeed equivalent to the term $\varepsilon + \pi_o$ derived by Philip (1958b) from cell water relations theory.

5.2. Local equilibrium and composite tissue models

Based on our analyses, local equilibrium between cell apoplast and symplast, and the air in adjacent pore spaces, appears to be a reasonable starting assumption for investigation of leaf transport properties averaged over whole leaves. Our conclusions regarding local equilibrium differ somewhat from Molz (1976), Molz et al. (1979), who suggested LE between protoplasts and their walls might be assumed to be the rule rather than the exception in most plant tissues, except perhaps in leaves, due to the potentially short path lengths that might exist there for flow. However, with the updated parameter values considered here, the analytic criteria we develop (Eq. (39)) supports LE with $k_s/k_a \approx 0.1$ even over cell files only 2–3 cells long.

We also found that, while LE and the error associated with the composite model are indeed linked as Molz suggested, the relationship is sensitive to the geometry and ratio of hydraulic capacities. For example, in the thick-walled case, we saw that the composite model continues to do well even as LE breaks down during the transient, such that its tolerance of divergences in magnitude between apoplastic and symplastic hydraulic conductivities is similar to that of the thin walled case. However, in files of cells with air spaces the composite model proved less robust than LE as $k_v > k_l$. The difference is due to the vanishingly small hydraulic capacity of the air relative to the cells.

Nevertheless, the fact that the isothermal hydraulic conductivity of the gas phase coincides with the low end of the range expected for cells, suggests that errors arising from composite model may be generally expected to be less than 10%. In the event $k_l > k_v$, the liquid phase material properties dominate the behavior of the system, and the composite description is simply $\kappa_\ell = \mathcal{A}_l k_l / \mathcal{V}_l c_l$. Yet, should the fits form the composite model to real data result in an estimate of hydraulic conductivity for the tissue, k_ℓ, far below that of air, then the assumption of LE should be re-examined, as we have shown the composite description breaks down for $k_l/k_v < 0.1$.

While we have only explicitly considered the chemical equilibrium of water molecules, the thermal and chemical problems have the same mathematical structure, and so the analysis may be expected to be similar. As the thermal conductivity of air is an order of magnitude less than that of liquid phase, whose thermal conductivity may be expected to be of the same order of magnitude as water (Vogel, 1983), and because the thermal capacity of air is likewise an order of magnitude lower than that of water, the case for a composite model for heat transport would appear to be stronger than for water molecules. The gas phase cannot 'short circuit' the liquid phase heat flux, as it might if the thermal conductivity of air were very high; nor will it provide a large lateral impedance, as the combination of high thermal capacity and low conductivity might, which would slow the time for heat transport from what might be expected based on the composite model. The thermal diffusivity of the composite will then just be dominated by that of the liquid fraction, or $\kappa_\ell^T = \mathcal{A}_l k_l^T / \mathcal{V}_l c_l^T$, where the superscript T refers to thermal properties.

5.3. Pathway of isothermal water flux in leaf tissue

With regard to the competition between isothermal vapor and liquid transport within a tissue, all of our estimates of k_l exceed k_v, though the low end of the k_s distribution for individual protoplasts is comparable. Experimental estimates of k_ℓ greater than $\sim 2 \times 10^{-13}$mol m^{-1} Pa^{-1} s^{-1} would suggest a dominant role for liquid flow over vapor diffusion. Mott and Peak (2011) proposed that vapor diffusion might be more important than liquid flow for transport through the mesophyll under isothermal (dark) conditions in leaves of *Tradescantia*, but based on a k_s 1.6×10^{-12} mol m^{-1} Pa^{-1} s^{-1}, estimated earlier from data in Ye et al. (2008), our estimate of k_v, and a whole leaf volumetric air fraction of 15% (Byott, 1976), this would appear unlikely.

While the non-isothermal case is beyond the scope of this paper, temperature gradients within the leaf have the potential to

shift more of the flux into the vapor phase than is predicted to occur in the isothermal case developed here. An idea of the difference can be gained by considering (64). At 25 °C, $c_v^\theta = 0.075$ mol m^{-3} K^{-1}, and the ratio c_v^θ/c_v^θ indicates that thermal gradients within leaf tissue of 0.1 °C, the order of magnitude expected for leaves (Yianoulis and Tyree, 1984), are as efficient at moving water as liquid phase gradients on the order of 1 MPa. In addition, while to define average tissue hydraulic properties from experiments we needed the volumetric air fraction averaged over the entire leaf, the appropriate air fraction for considering the transpirational flux between the veins and lower epidermis is that of the spongy mesophyll, further contributing to the competitiveness of the vapor phase. These issues will be further explored in a subsequent analysis.

The important point with regard to the experimental determination of material properties is that as long as rehydration experiments are conducted at a temperature close to transpiring 'leaf temperatures' (i.e., the temperature measured by a thermocouple at the leaf surface), the isothermal value of k_l should still be appropriate for modeling liquid phase transport under non-isothermal conditions. This is because temperature variations in the leaf are expected to be less than <1 °C, while the conductivity of the cell fraction is thought to have a Q10 of about 2 (Matzner and Comstock, 2001), from which it follows we can safely neglect variation in k_l due to temperature gradients within a leaf.

With the respect to the question of whether most of the liquid flux in the leaf mesophyll occurs through the walls or symplast, for the thin wall aspect ratio considered here, $w_a/l_c = 0.01$, we found that even for ratios of the symplast to apoplast hydraulic conductivity of $k_s/k_a > 0.05$ the steady flux across the symplast will be larger, simply due to the relatively small area available for apoplastic flow. Experimental values of k_l on the order of 10^{-11} mol m^{-1} Pa^{-1} s^{-1} would be higher than could be explained by the symplastic path, based on the estimates of k_s given here. Such values, if observed, would support the concept of a predominantly apoplastic path in leaf mesophyll tissue, as some work on leaves assumes (Brodribb et al., 2007, 2010). Despite this assumption, the fit to the data in Brodribb et al. (2007, Fig. 1B) implies a universal k_ℓ for ferns, gymnosperms, angiosperms, and lycopods of 2×10^{-12} mol m^{-1} Pa^{-1} s^{-1}, which may readily be accounted for by the estimates of k_s based on pressure probe estimates of L_p given here. Thus it seems unnecessary to invoke a large apoplastic flux to account for water transport in leaf tissue.

According to Martre et al. (2002), in *Arabidopsis* estimates of L_p of this magnitude, $\sim10^{-13}$ m Pa^{-1} s^{-1}, correspond to $P_{os} > 10$ μm s^{-1} that are indicative of active aquaporins. L_P measurements from pressure probes do not discriminate between cross-membrane and plasmodesmatal mediated fluxes, so it is notable that P_{os} values appear capable of accounting for the magnitude of observed cell-to-cell conductivities. An important role for aquaporins within the symplastic compartment is also consistent with the negative effect of anoxia, known to gate aquaporins (Tournaire-Roux et al., 2003), on the rehydration of *Quercus rubra* leaves (Rockwell et al., 2011).

It is perhaps surprising then that Martre et al. (2002) found no effect of down regulation of aquaporins on leaf hydraulic conductance, defined as the proportionality between transpiration and the difference between covered leaf (presumably in equilibrium with the stem xylem) and transpiring leaf water potentials, while an effect was seen in roots. Martre et al. conclude these results are consistent with a dominantly apoplastic path for transpiration. However, while the potential difference driving flow across the root was well defined in that study, the relationship between whole leaf volume averaged water potential measurements and the potential at the evaporation sites in leaves is not (Sack et al., 2002).

Evaporative methods can also give highly nonlinear potential-flux relations, in which the potential differences between transpiring and non-transpiring leaves appears insensitive to increases in the flux, a problem particularly for measurements of detached leaves of young, growing herbaceous plants (Boyer, 1985). In addition, the potential difference between transpiring and non-transpiring leaves may be well-defined in plants in which xylem resistance is much greater than the post-xylem path through the tissue, such that all the living tissue in the leaf may be approximated as at one potential, but, in the case of angiosperms, tissue resistance is not negligible (Cochard et al., 2004). As a result, the capacitance of tissue not between the minor veins and the stomata (e.g., palisade and upper epidermis in hypostomatous leaves, rib tissues) will reduce the sensitivity of the average potential of the leaf, as measured by the pressure chamber, to changes in vein to stomata gradients. While attractive for characterizing flux–potential relations at phylogenetic scales (e.g., Brodribb et al., 2007), evaporative methods do not appear sufficiently well-defined physically to probe finer scale leaf structure-function relationships. In the case of Martre et al. (2002), the method may simply have been to crude to detect a change in leaf tissue permeability.

In conclusion, our analysis has shown that all of the pathways considered here, apoplastic, symplastic, and through the air spaces as vapor, may be important for water transport within a particular tissue depending on the volume fractions, wall thicknesses, and temperature gradients that characterize the tissue. Modeling the path of transpiration in leaf tissues should therefore take all of these factors into account. Yet while the topology of the walls, protoplasts and air spaces is complex, a simple composite model of leaf tissue as a homogenous isotropic medium characterized by the area and volume averaged material properties of the component sub-domains appears to offer a good working hypothesis or starting point for exploring leaf structure-function relationships related to water transport.

Appendix A. Sensitivity of poroelastic relaxation times to ν

The solution to diffusion type boundary value problems can be expressed at any particular time as a sum of n exponential terms, where the contribution to the solution of any particular term decays as both $n\to\infty$ and $t\to\infty$ (Crank, 1957). As a result, at 'long times,' or after about one quarter of the progress of the transient to the final equilibrium state has occurred, the solution maybe well described by a single dominant term. While no closed form solution to the free swelling linear poroelastic problem exists, Doi (2009) sketches the expected form of the longest relaxation time, which will determine the half time of the swelling kinetics. According to Doi's (2009) solution, the time constant τ_o of the dominant term, or 'longest relaxation time,' is given by (in our notation, with $L=h/2$),

$$\tau_o = \frac{L^2}{\kappa\lambda^2}, \quad \kappa = \overline{v}\left(\frac{3K(1-\nu)}{1+\nu}\right)k, \tag{A.1}$$

where λ is the smallest positive solution to,

$$\lambda\cot\lambda = \frac{4G}{3K+4G} = \frac{2(1-2\nu)}{1-\nu}. \tag{A.2}$$

Note that the second equality simply follows from the relationship between G and K given by (11). Inspection of (A.(1) and A.2) shows that, for a given hydraulic conductivity k and volumetric modulus K, the longest relaxation time τ_o is just a function of the poroelastic Poisson's ratio, ν. For $\nu=0.1$ and $\nu=0.5$, the longest relaxation

times are calculated as,

$$\tau_o(\nu=0.1)=\frac{0.362L^2}{\overline{\nu}Kk},\quad \tau_o(\nu=0.5)=\frac{4L^2}{\pi^2\overline{\nu}Kk}. \tag{A.3}$$

With $4/\pi^2\approx 0.405$, the difference between the longtime solutions for the two values of ν is 12%. We also see that the $\nu=0.5$ case conforms to the longtime solution for potential diffusion into a plane sheet, with the permeable surface at $x=0$, no-flux by symmetry at the mid-plane at $x=L$, and $c\equiv 1/\overline{\nu}K$ (Crank, 1957),

$$\frac{\psi(t)-\psi_\infty}{\psi_o-\psi_\infty}\approx\frac{8}{\pi^2}\exp\left(-\frac{\pi^2 k}{4cL^2}t\right). \tag{A.4}$$

This is indeed for the above boundary conditions the longtime solution to (12), the heat-equation form we found the equations of poroelasticity reduce to in the special case $\nu=0.5$, equivalent to Philip's (1958b) model (8).

Appendix B. Relating osmotic and potential flows

The relationship between P_{os}, the permeability defined by protoplast swelling assays, and L_p, the hydraulic permeability as measured by the pressure probe, can be found by relating the absolute volume fluxes (Boyer, 1995; Ramahaleo et al., 1999),

$$\frac{\partial v}{\partial t}=P_{os}S_o\cdot\overline{\nu}\rho_w\Delta C_{os}=L_pS_o\cdot\Delta\psi, \tag{B.1}$$

where S_o is the initial surface area of the protoplast, and C_{os} is the osmolality, in mol/kg solvent, as reported in Ramahaleo et al. In the limit of dilute solutions, $\rho_w C_{os}$ gives the concentration C in mol/m^3, and $\overline{\nu}\rho_w C_{os}$ the dimensionless mole fraction, that describe the osmotic difference driving flow across the membrane. Using the relationship between dilute concentrations and water potential, $\psi_\pi=-RTC$ (Kramer and Boyer, 1995), and recognizing that the 'positive' differences in C_{os} and ψ driving inward flow have opposite signs when written more formally as gradients, leads to,

$$\frac{\Delta C_{os}}{\Delta\psi}=(\rho_w RT)^{-1}\rightarrow L_p=\frac{P_{os}\overline{\nu}}{RT}. \tag{B.2}$$

Appendix C. Approximately isothermal vapor transport

Here we consider vapor transport within the leaf tissue, in the absence of radiative loading of the leaf. Because of the low capacity of air for water molecules relative to the cells, effectively all of the water entering the leaf in the liquid phase during a hydration experiment ultimately resides in the cells, again in the liquid phase. This means that to the extent water moves through the internal air space as vapor during a change in hydration, energy must flow towards the evaporative surfaces (i.e., the bundle sheath) as well as away from the condensing and absorbing cells in the mesophyll and epidermis. Only if the amount of energy removed by evaporation is small relative to the heat capacity of the tissue, will temperature variations at the evaporating and condensing sites truly be negligible. Yet, if we treat the entire tissue (noting that the heat capacity of the air fraction is negligible compared to that of water) as a reservoir of heat energy, we find that for a typical oak leaf containing 1.2 g of water in a typical hydration experiment that results in the uptake of 0.04 g, or $\sim 3\%$ of the leaf's water content, the energy required to evaporate the hydration flux relative to the energy required to change temperature of the leaf water 1 °C is,

$$\frac{\overline{\lambda}}{c_p}\cdot 0.03\approx 17.5\ ^\circ\mathrm{C}, \tag{C.1}$$

which tells us that, in the absence of a flow of energy to the evaporation sites, the thermal gradients induced in the tissue by a vapor flux would not be negligible. Of course, in the absence of radiative loading from an external source, energy can flow to the leaf from the surrounding air, but this potential source is separated from the leaf tissue by a conductive boundary layer resistance.

A more important source of energy is likely to be the sites of condensation within the leaf itself. To estimate how important thermal gradients might then be in slowing vapor transport, we can find an approximate thermally 'corrected' hydraulic conductivity of the air by imposing the requirement (which would be exact in steady state) that any latent heat transport must be conducted back to the evaporating site a distance Δx away. In terms of the latent heat flux that arises due to vapor transport in the air fraction $\mathcal{A}_v$ during rehydration, the conduction of heat through the leaf tissue required to deliver the heat of condensation back to the evaporative surface is given by,

$$\mathcal{A}_v\overline{\lambda}J_v=k_\ell^T\frac{\Delta\theta}{\Delta x}, \tag{C.2}$$

where k_ℓ^T, the thermal conductivity of the leaf, is given by $\mathcal{A}_l k_l^T+\mathcal{A}_v k_v^T$. Solving (C.2) for the temperature gradient (induced by vapor transport and driving heat transport from the site of condensation back to the site of evaporation), and substituting back into (64), we find an expression for the vapor flux in the air space that accounts for the adverse impact of a temperature gradient on vapor transport,

$$J_v=-D_v c_v^\psi\frac{\partial\psi}{\partial x}-D_v c_v^\theta\frac{\mathcal{A}_v\overline{\lambda}J_v}{k_\ell^T}. \tag{C.3}$$

Re-arranging (C.3) defines an effective hydraulic conductivity of the air space, k_v^*, that takes into account thermal effects,

$$J_v=-k_v^*\frac{\partial\psi}{\partial x},\quad k_v^*=\frac{D_v c_v^\psi}{1+D_v c_v^\theta\dfrac{\mathcal{A}_v\overline{\lambda}}{k_\ell^T}}. \tag{C.4}$$

For an oak leaf with a tissue thermal conductivity about a third that of water, or 0.25 J m^{-1} K^{-1} s^{-1}, and a whole leaf air fraction of 12.63% (unpublished data), the correction amounts to only a 4% reduction in the hydraulic conductivity of the vapor path, a result due to the efficiency of conduction in the leaf tissue relative to vapor transport. A full thermal budget would also account for convective heat transport as well as radiative transfer across the air spaces; it can be shown these are negligible effects, but formal development of the arguments will be left to a more complete description of non-isothermal water transport in leaves, in preparation.

References

Biot, M., 1941. General theory of three-dimensional consolidation. Journal of Applied Physics 12, 155–164.

Bird, R.B., Stewart, W.E., Lightfoot, E.N., 1960. Transport Phenomena. John Wiley & Sons, New York, NY.

Boyce, C.K., Brodribb, T.J., Feild, T.S., Zwieniecki, M.A., 2009. Angiosperm leaf vein evolution was physiologically and environmentally transformative. Proceedings of the Royal Society B 276, 1771–1776.

Boyer, J.S., 1968. Relationship of leaf water potential to leaf growth. Plant Physiology 43, 1056–1062.

Boyer, J.S., 1985. Water transport. Annual Review of Plant Physiology 36, 473–516.

Boyer, J.S., 1995. Measuring the Water Status of Plants and Soils. Academic Press, San Diego, CA.

Brodribb, T.J., Feild, T.S., Jordan, G.J., 2007. Leaf maximum photosynthetic rate and venation are linked by hydraulics. Plant Physiology 144, 1890–1898.

Brodribb, T.J., Feild, T.S., Sack, L., 2010. Viewing leaf structure and evolution from a hydraulic perspective. Functional Plant Biology 37, 488–498.

Brodribb, T.J., Holbrook, N.M., 2003. Stomatal closure during leaf dehydration, correlation with other leaf physiological traits. Plant Physiology 132, 2166–2173.

Burgert, I., 2006. Exploring the micromechanical design of plant cell walls. American Journal of Botany 93, 1391–1401.

Byott, G., 1976. Leaf air space systems in c3 and c4 species. New Phytologist 76, 295–299.
Cai, S., Hu, Y., Zhao, X., Suo, Z., 2010. Poroelasticity of a covalently crosslinked alginate hydrogel under compression. Journal of Applied Physics 108, 113514.
Carslaw, H., Jaeger, J., 1959. Conduction of Heat in Solids. Oxford University Press, New York, NY.
Cochard, H., Nardini, A., Coll, L., 2004. Hydraulic architecture of leaf blades: where is the main resistance?. Plant, Cell and Environment 27, 1257–1267.
Cochard, H., Venisse, J.S., Barigah, T.S., Brunel, N., Herbette, S., Guilliot, A., Tyree, M.T., Sakr, S., 2007. Putative role of aquaporins in variable hydraulic conductance of leaves in response to light. Plant Physiology 143, 122–133.
Cosgrove, D., 1988. In defence of the cell volumetric elastic modulus. Plant, Cell and Environment 11, 67–69.
Crank, J., 1957. The Mathematics of Diffusion. Oxford University Press, New York, NY.
Cussler, E.L., 1997. Diffusion, Mass Transfer in Fluid Systems, 2nd edition Cambridge University Press, Cambridge, UK.
Deen, W.M., 1998. Analysis of Transport Phenomena. Oxford University Press, New York, NY, USA.
Doi, M., 2009. Gel dynamics. Journal of the Physical Society of Japan 78, 052001.
Esau, K., 1960. Anatomy of Seed Plants, 2nd edition John Wiley & Sons, New York, NY, USA.
Gandar, P., 1983. Growth in root apices 1. The kinematic description of growth. Botanical Gazette 144, 1–10.
Hong, W., Zhao, X., Zhou, J., Suo, Z., 2008a. A theory of coupled diffusion and large deformation in polymeric gels. Journal of the Mechanics and Physics of Solids 56, 1779–1793.
Hong, W., Zhao, X., Zhou, J., Suo, Z., 2008b. A theory of coupled diffusion and large deformation in polymeric gels. Journal of the Mechanics and Physics of Solids 56, 1779–1793.
Johnson, D.M., Woodruff, D., McCulloh, K., Meinzer, F., 2009. Leaf hydraulic conductance, measured in situ, declines and recovers daily: leaf hydraulics, water potential and stomatal conductance in four temperate and three tropical tree species. Tree Physiology 29, 879–887.
Kim, Y.X., Steudle, E., 2007. Light and turgor affect the water permeability (aquaporins) of parenchyma cells in the midrib of leaves of Zea mays. Journal of Experimental Botany 58, 4119–4129.
Kramer, P., Boyer, J.S., 1995. Water Relations of Plants and Soils. Academic Press, San Diego, CA.
Martre, P., Morillon, R., Barrieu, F., North, G., Nobel, P., Chrispeels, M., 2002. Plasma membrane aquaporins play a significant role during recovery from water deficit. Plant Physiology 130, 2101–2110.
Matzner, S., Comstock, J., 2001. The temperature dependence of shoot hydraulic resistance: implications for stomatal behaviour and hydraulic limitation. Plant, Cell and Environment 24, 1299–1307.
Michael, W., Schultz, A., Meshcheryakov, A., Ehwald, R., 1997. Apoplasmic and protoplasmic water transport through the parenchyma of the potato storage organ. Plant Physiology 115, 1089–1099.
Molz, F., 1976. Water transport through plant tissue: the apoplasm and symplasm pathways. Journal of Theoretical Biology 59, 277–292.
Molz, F., Ikenberry, E., 1974. Water transport through plant cells and cell walls: theoretical development. Soil Science Society of America Journal 38, 699.
Molz, F., Kerns Jr., D., Peterson, C., Dane, J., 1979. A circuit analog model for studying quantitative water relations of plant tissues. Plant Physiology 64, 712.
Morillon, R., Chrispeels, M., 2001. The role of ABA and the transpiration stream in the regulation of the osmotic water permeability of leaf cells. Proceedings of the National Academy of Sciences of the United States of America 98, 14138–14143.
Mott, K.A., Peak, D., 2011. A new, vapour-phase mechanism for stomatal responses to humidity and temperature. Plant, Cell and Environment 34, 162–178.
Niklas, K., 1992. Plant Biomechanics: An Engineering Approach to Plant Form and Function. Chicago University Press, Chicago, IL.
Nobel, P.S., 2005. Physicochemical and Environmental Plant Physiology. Elsevier Academic Press, Burlington, MA, USA.
Philip, J., 1958a. The osmotic cell, solute diffusibility, and the plant water economy. Plant Physiology 33, 264–271.
Philip, J., 1958b. Propagation of turgor and other properties through cell aggregations. Plant Physiology 33, 271–274.
Pieruschka, R., Huber, G., Berry, J., 2010. Control of transpiration by radiation. Proceedings of the National Academy of Sciences of the United States of America 107, 13372–13377.
Pieruschka, R., Schurr, U., Jahnke, S., 2005. Lateral gas diffusion inside leaves. Journal of Experimental Botany 56, 857–864.
Ramahaleo, T., Morillon, R., Alexandre, J., Lassalles, J., 1999. Osmotic water permeability of isolated protoplasts. Modifications during development. Plant Physiology 119, 885–896.
Rockwell, F.E., Holbrook, N.M., Stroock, A. 2013. Leaf hydraulics II: vascularized tissues. Journal of Theoretical Biology, http://dx.doi.org/10.1016/j.jtbi.2013.08.027.
Rockwell, F.E., Holbrook, N.M., Zwieniecki, M.A., 2011. Hydraulic conductivity of red oak (*Quercus rubra L.*) leaf tissue does not respond to light. Plant, Cell and Environment 34, 565–579.
Sack, L., Melcher, P.J., Zwieniecki, M.A., Holbrook, N.M., 2002. The hydraulic conductance of the angiosperm leaf lamina: a comparison of three measurement methods. Journal of Experimental Botany 53, 2177–2184.
Scoffoni, C., Pou, A., Aasamaa, K., Sack, L., 2008. The rapid light response of leaf hydraulic conductance: new evidence from two experimental methods. Plant, Cell and Environment 31, 1803–1812.
Tournaire-Roux, C., Sutka, M., Javot, H., Gout, E., Gerbeau, P., Luu, D.T., Bligny, R., Maurel, C., 2003. Cytosolic pH regulates root water transport during anoxic stress through gating of aquaporins. Nature 425, 393–397.
Vogel, S., 1983. The lateral thermal conductivity of leaves. Canadian Journal of Botany 62, 741–744.
Wylie, R.B., 1939. Relations between tissue organization and vein distribution in dicotyledon leaves. American Journal of Botany 26, 219–225.
Ye, Q., Holbrook, N.M., Zwieniecki, M.A., 2008. Cell-to-cell pathway dominates xylem-epidermis hydraulic connection in *Tradescantia fluminensis* (Vell. Conc.) leaves. Planta 227, 1311–1319.
Yianoulis, P., Tyree, M.T., 1984. A model to investigate the effect of evaporative cooling on the pattern of evaporation in sub-stomatal cavities. Annals of Botany 53, 189–206.
Yoon, J., Cai, S., Suo, Z., Hayward, R.C., 2010. Poroelastic swelling kinetics of thin hydrogel layers: comparison of theory and experiment. Soft Matter 6, 6004–6012.